

5-2017

# Optimization of A Combined Carbon/Oxygen And Neutron Porosity Oil Well Logging Tool

Entisar Ali Al Muraikhi

Follow this and additional works at: [https://scholarworks.uaeu.ac.ae/all\\_theses](https://scholarworks.uaeu.ac.ae/all_theses)

Part of the [Physics Commons](#)

---

## Recommended Citation

Al Muraikhi, Entisar Ali, "Optimization of A Combined Carbon/Oxygen And Neutron Porosity Oil Well Logging Tool" (2017).  
*Theses*. 624.

[https://scholarworks.uaeu.ac.ae/all\\_theses/624](https://scholarworks.uaeu.ac.ae/all_theses/624)

This Thesis is brought to you for free and open access by the Electronic Theses and Dissertations at Scholarworks@UAEU. It has been accepted for inclusion in Theses by an authorized administrator of Scholarworks@UAEU. For more information, please contact [fadl.musa@uaeu.ac.ae](mailto:fadl.musa@uaeu.ac.ae).



جامعة الإمارات العربية المتحدة  
United Arab Emirates University

United Arab Emirates University

College of Science

Department of Physics

OPTIMIZATION OF A COMBINED CARBON/OXYGEN AND  
NEUTRON POROSITY OIL WELL LOGGING TOOL

Entisar Ali AL Muraikhi

This thesis is submitted in partial fulfillment of the requirements for the degree  
Master of Science in Physics

Under the Supervision of Professor Nacir M. Tit

May 2017

### Declaration of Original Work

I, Entisar Ali AL Muraikhi, the undersigned, a graduate student at the United Arab Emirates University (UAEU), and the author of this thesis entitled "*Optimization of a Combined Carbon/Oxygen and Neutron Porosity Oil Well Logging Tool*", hereby, solemnly declare that this thesis is my own original research work that has been done and prepared by me under the supervision of Professor Nacir M. Tit, in the College of Science at UAEU. This work has not previously been presented or published, or formed the basis for the award of any academic degree, diploma or a similar title at this or any other university. Any materials borrowed from other sources (whether published or unpublished) and relied upon or included in my thesis have been properly cited and acknowledged in accordance with appropriate academic conventions. I further declare that there is no potential conflict of interest with respect to the research, data collection, authorship, presentation and/or publication of this thesis.

Student's Signature: \_\_\_\_\_

انتصار المرعي

Date: \_\_\_\_\_

24/5/2017

Copyright © 2017 Entisar Ali Al Muraikhi  
All Rights Reserved

## **Advisory Committee**

1) Advisor: Prof. Nacir M. Tit

Title: Professor

Department of Physics

College of Science

UAE University

2) Co-advisor: Dr. Walid Metwally

Title: Associate Professor

Department of Nuclear Engineering

College of Engineering

University of Sharjah

## Approval of the Master Thesis

This Master Thesis is approved by the following Examining Committee Members:

- 1) Advisor (Committee Chair): Prof. Nacir M. Tit

Title: Professor

Department of Physics

College of Science, UAEU

Signature 

Date 21/5/2017

- 2) Member: Prof. Nouredine Amrane

Title: Professor

Department of Physics

College of Science, UAEU

Signature 

Date 21/5/2017

- 3) Member (External Examiner): Prof. Attaelmanan Gaffar

Title: Professor

Department of Applied Physics and Astronomy

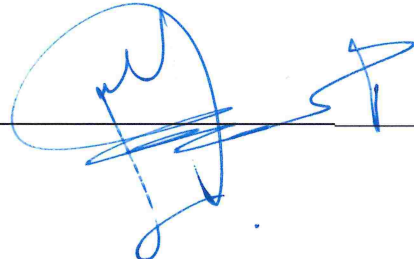
College of Science, University of Sharjah

Signature 

Date 17/5/2017

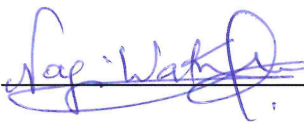
This Master Thesis is accepted by:

Dean of the College of Science: Professor Ahmed Ali Murad

Signature 

Date 24/5/2017

Dean of the College of Graduate Studies: Professor Nagi T. Wakim

Signature 

Date 24/5/2017

## Abstract

Well logging technique is used to determine the physical and chemical properties of borehole formation, by using neutron porosity oil well logging tools. The present study simplifies logging tool design in order to reduce the time spent on obtaining well logging. We have combined both carbon/oxygen (C/O) tool and thermal neutron porosity tool. This has been done by adding boron lining on the detectors in C/O tool, where the boron lining acts as a thermal neutron porosity tool while maintaining C/O functions simultaneously. The Monte Carlo N-Particle (MCNP) Transport Code, which was originally developed in Los Alamos National Laboratory, is used to investigate the combined tool response. The combined tool is employed to detect the effect of porosity. The effects of several factors, such as (i) the source-to-detector spacing, (ii) borehole salinity, (iii) capture cross section, (iv) boron lining thickness, (v) formation salinity, (vi) borehole salinity, (vii) temperature, and (viii) the casing on the detection sensitivity are investigated. The results show that the number of detected gamma rays is proportional to the porosity. Furthermore, a sensitivity measure (i.e., the sensitivity ratio) is defined and used to characterize the detectors sensitivity to the porosity. The effects of various factors on the sensitivity are studied and the response function is found to be very sensitive to the porosity especially in the domain of low values of it. The temperature factor was only examined to assess its effect on the nucleus speed. However, the results of our simulations showed that the temperature has very little minor effect. Evidently, the tool is sensitive to the porosity while maintaining all the functions of the C/O tool, which suggests that the boron lining can efficiently serve as a replacement of the porosity tool.

**Keywords:** Well logging, C/O tool, thermal-neutron-porosity tool, boron lining, MCNP package, combined tool, porosity, sensitivity measure.



## Title and Abstract (in Arabic)

### تحسين تصميم أداة موحدة في رصد الآبار البترولية والمؤلفة من أداة الكربون / الأكسجين وأداة قياس المسام باستخدام النيوترونات

#### الملخص

تم استخدام تقنية رصد الآبار لتحديد الخواص الفيزيائية والكيميائية لتكوين البئر، وذلك باستخدام أدوات رصد الآبار البترولية للمسام بإستعمال النيوترونات. تهدف هذه الدراسة إلى تبسيط تصميم أداة رصد الآبار من أجل تقليل الوقت المستغرق في رصد الآبار، وقد يجمع الباحث بين أداة الكربون/أكسجين و أداة قياس المسام بإستعمال النيوترونات ذات الطاقة المنخفضة. قد تم ذلك بإضافة بطانة مادة البورون على أجهزة الكشف في أداة الكربون/أكسجين، حيث تعمل بطانة البورون دور أداة قياس المسام باستخدام النيوترونات ذات الطاقة المنخفضة، مع الحفاظ على وظائف أداة الكربون/أكسجين في الوقت نفسه. يستخدم برنامج محاكاة المونتي كارلو لجسيم النيوترون، والذي تم تطويره في المختبر الوطني لوس ألاموس للتحقق من استجابة الأداة الموحدة. استخدمت الأداة الموحدة للكشف عن تأثير المسام وعوامل أخرى على حساسية الكشف، مثل 1- بعد المصدر عن الكاشف، 2- سمك البطانة، 3- حجم البئر، 4- ملوحة البئر، 5- ملوحة التكوين، 6- درجة الحرارة، 7- احتمالية الأسر، 8- والغلاف. أظهرت النتائج أن أشعة جاما المنبعثة تتناسب مع المسامية. و علاوة على ذلك، فقد تم تعريف مقياس الحساسية المستخدم (أي نسبة الحساسية) لوصف حساسية أجهزة الكشف للمسامية، وقد وصفت تأثير هذه العوامل على الحساسية لتكون الاستجابة أكثر حساسية عند القيم الصغيرة للمسامية، بينما تمت دراسة عامل درجة الحرارة فقط لتحديد تأثيره على سرعة النواة، وأظهرت نتائج المحاكاة أن درجة الحرارة ليس لها تأثير.

نستنتج من ذلك أن الأداة الموحدة حساسة للمسامية على الغالب مع الحفاظ على وظائف أداة الكربون/أكسجين، وبالتالي فإن بطانة البورون يمكن أن تعمل بكفاءة كبديل لأداة المسامية.

**مفاهيم البحث الرئيسية:** رصد الآبار، أداة قياس نسبة الكربون/الأكسجين، أداة قياس المسام باستخدام النيوترونات ذات الطاقة المنخفضة، بطانة البورون، المونت كارلو للنيوترونات الجسيمية، الأداة الموحدة، المسام، قياس الحساسية.

## **Acknowledgements**

First, I thank God for completing this research, and I am especially grateful to my academic Co-advisor Dr. Walid Metwally, Associated Professor in the Department of Engineering/University of Sharjah, for his support, advice, guidance and encouragement along the hard process of the preparation of this thesis. I would like to thank my committee for their guidance, support, and assistance throughout my preparation of this thesis, especially my advisor Prof. Nacir M. Tit who agreed to co-supervise my thesis. I would like to thank the chairman and all members of the Department of Physics at the United Arab Emirates University, especially Prof. Usama Al-Khawaja, and Prof. Abdessamad Abada. My special thanks are extended to the Library Research Desk for providing me with the needed reference materials.

Special thanks go to my parents, brothers, and sisters who have extended their unlimited help. In addition, special thanks are extended to the Al Muraikhi family for their moral supports.

## **Dedication**

*To my beloved U.A.E*

## Table of Contents

Title.....	i
Declaration of Original Work.....	ii
Copyright.....	iii
Advisory Committee.....	iv
Approval of the Master Thesis .....	v
Abstract .....	vii
Title and Abstract (in Arabic) .....	viii
Acknowledgements.....	ix
Dedication .....	x
Table of Contents.....	xi
List of Tables.....	xiii
List of Figures.....	xiv
List of Abbreviations .....	xvi
Chapter 1: Introduction .....	1
1.1 Overview.....	1
1.2 Prompt Gamma-Ray Neutron Activation Analysis.....	1
1.3 Well Logging Tools.....	2
1.3.1 Neutron-Porosity Logging Tool.....	3
1.3.2 C/O Logging Tool .....	3
1.4 Neutron Source.....	3
1.5 Well Logging Tool Detectors' Types.....	4
1.5.1 Sodium Iodide Detector .....	5
1.6 Statement of the Problem.....	6
1.7 Introduction to Monte Carlo N-Particle Simulation.....	6
1.8 Relevant Literature .....	7
1.9 Conception .....	15
Chapter 2: Methods.....	17
2.1 Combined Tool Design.....	17
2.2 Thermal Neutron Interaction with Boron .....	18
2.3 The Effect of the Source-to-Detector Spacing on the Combined Tool Response .....	19
2.4 The Effect of Casing (Stainless Steel) Thickness on the Combined Tool Response .....	19
2.5 The Effect of the Borehole Size on the Combined Tool Response.....	19
2.6 The Effect of the Temperature on the Combined Tool Response.....	20
2.7 The Effect of the Cross Section on the Combined Tool Response .....	20
2.7.1 Attenuation of Gamma-Rays .....	22
2.7.2 Types of Neutron Interactions with Matter.....	22
2.7.3 Neutron Cross Section [ $\sigma(\text{m}^2)$ ].....	23
2.7.4 Macroscopic Cross Section [ $\Sigma (\text{m}^{-1})$ ] .....	24
2.7.5 Mean Free Path [ $\lambda(\text{m})$ ].....	24

2.8 The Effect of the Borehole Salinity on the Combined Tool Response .....	24
2.8.1 Calculation of Density and Weight Fraction .....	24
2.9 The Effect of the Formation Salinity on the Combined Tool Response ....	26
2.10 The Effect of the Boron Thickness on the Combined Tool Response .....	27
2.11 Calculation of the Sensitivity Ratio.....	27
2.11.1 Calculation of the Sensitivity Error .....	28
Chapter 3: Results.....	29
3.1 The Effect of Porosity on the Combined Tool Response .....	29
3.1.1 The Effect of Porosity on the Limestone Density .....	29
3.1.2 Calculation of Weight Fraction for Formation Elements .....	30
3.2 Calculation of Error .....	31
3.3 The Reduction of the Neutron Flux Incident on the Detectors .....	38
3.4 Factors Affecting on the Combined Tool Response Results .....	41
3.4.1 Source-to-Detector Spacing Results.....	41
3.4.2 Casing (Stainless Steel) Thickness Results .....	42
3.4.3 Borehole Size Results .....	44
3.4.4 Temperature Results .....	45
3.4.5 Cross Section Results .....	46
3.4.6 Borehole Salinity Results.....	47
3.4.7 Formation Salinity Results.....	49
3.4.8 Boron Thickness Results .....	51
3.5 Sensitivity Results .....	53
Chapter 4: Discussion .....	56
4.1 Interpretation of the Effect of the Porosity on the Combined-Tool Response .....	56
4.2 Interpretation of the Reduction of the Incident Neutron Flux on the Detectors .....	57
4.3 Interpretation of Factors Affecting the Combined Tool Response .....	58
4.3.1 Source-to-Detector Spacing Factor Results .....	58
4.3.2 Casing (Stainless Steel) Thickness Factor Results.....	59
4.3.3 Borehole Size Factor Results .....	59
4.3.4 Temperature Factor Results .....	60
4.3.5 Cross Section Factor Results.....	60
4.3.6 Borehole Salinity Factor Results.....	60
4.3.7 Formation Salinity Factor Results.....	61
4.3.8 Boron Thickness Factor Results.....	61
Chapter 5: Conclusion.....	63
References .....	64

## List of Tables

Table 1: Variation of Limestone Density versus Porosity .....	29
Table 2: Output File of Near Detector Counts .....	32
Table 3: Near Detector Counts .....	33
Table 4: Far Detector Counts .....	33
Table 5: Normalized Ratio with Error versus Porosity.....	37
Table 6: Density of Saline Water versus Salinity.....	48
Table 7: Formation Density versus Salinity and Porosity.....	50

## List of Figures

Figure 1: MCNP Design for Different Logging Tools [7].....	3
Figure 2: Sealed Tube Neutron Generator [10].....	4
Figure 3: NaI Detector [14].....	6
Figure 4: Monte Carlo Model of the Neutron-Porosity Tool with (a) an $x$ - $z$ view and (b) an $x$ - $y$ view .....	17
Figure 5: Neutron's Energy Versus Time [50].....	18
Figure 6: Neutron Beam Transmitted through the Absorber [52].....	21
Figure 7: Near Detector Counts.....	34
Figure 8: Far Detector Counts .....	34
Figure 9: Normalized Ratio of the Near to Far Detector Counts .....	35
Figure 10: Neutron Current in the Near Detector, Thermal Energy Range.....	39
Figure 11: Neutron Current in the Far Detector, Thermal Energy Range .....	39
Figure 12: Neutron Current in the Near Detector, Epithermal Energy Range.....	39
Figure 13: Neutron Current in the Far Detector, Epithermal Energy Range .....	40
Figure 14: Neutron Current in the Near Detector, Fast Energy Range.....	40
Figure 15: Neutron Current in the Far Detector, Fast Energy Range .....	40
Figure 16: Counts versus Porosity and Source-to-Detector Distance, Near Detector ....	41
Figure 17: Counts versus Porosity and Source-to-Detector Distance, Far Detector .....	41
Figure 18: Normalized Ratio versus Porosity and Source-to-Near Detector Distance ..	42
Figure 19: Count Rate versus Porosity and Casing-Thickness, Near Detector.....	42
Figure 20: Count Rate versus Porosity and Casing-Thickness, Far Detector .....	43
Figure 21: Normalized Count Ratio versus Stainless Steel Thickness.....	43
Figure 22: Count Rate versus Porosity and Borehole Size, Near Detector.....	44
Figure 23: Count Rate versus Porosity and Borehole Size, Far Detector .....	44
Figure 24: Normalized Count Ratio versus Borehole Size .....	45
Figure 25: Counts Rate versus Temperature, Near Detector .....	45
Figure 26: Counts Rate versus Temperature, Far Detector.....	46
Figure 27: Near Detector Counts versus Porosity for Two Different Cross Sections ....	46
Figure 28: Far Detector Counts versus Porosity for Two Different Cross Sections .....	47
Figure 29: Normalized Count Ratio versus Porosity for Two Different Cross Sections	47
Figure 30: Near Detector Counts, Borehole Salinity .....	48
Figure 31: Far Detector Counts, Borehole Salinity .....	49
Figure 32: Normalized Counting Ratio, Borehole Salinity.....	49
Figure 33: Near Detector Counts, Formation Salinity .....	50
Figure 34: Far Detector Counts, Formation Salinity .....	51
Figure 35: Normalized Counting Ratio, Formation Salinity.....	51
Figure 36: Photons Counts versus Porosity and Boron Thickness, Near Detector .....	52
Figure 37: Photons Counts versus Porosity and Boron Thickness, Far Detector.....	52
Figure 38: Normalized Count Ratio versus Porosity and Boron Thickness .....	53
Figure 39: Sensitivity Factor versus Porosity and the Source-to-Detector Spacing .....	53

Figure 40: Sensitivity versus Porosity and Casing Factor ..... 54  
Figure 41: Sensitivity versus Porosity and Borehole Size Factor ..... 54  
Figure 42: Sensitivity versus Porosity and Cross Section Factor..... 54  
Figure 43: Sensitivity versus Porosity and Borehole Salinity Factor ..... 55  
Figure 44: Sensitivity versus Porosity and Formation Salinity Factor ..... 55  
Figure 45: Sensitivity versus Porosity and Boron Thickness Factor ..... 55



### List of Abbreviations

ACTIA	Advanced Computational Technology Initiative
Am-B	Americium-Boron Source
Am-Be	Americium-Beryllium Neutron Source
b	Barn (the unit of cross section) is defined as the cross sectional area of a nucleus, where the nuclear radius around $10^{-15}$ - $10^{-14}$ m, $1b=10^{-24}\text{cm}^2=10^{-28}\text{m}^2$
BGO	Bismuth Germanium Oxide Compound
CaCO <sub>3</sub>	Limestone
<sup>252</sup> Cf	Californium-252 spontaneous fission source
<sup>60</sup> Co	Cobalt Isotope
C/O	(Carbon/Oxygen ) Ratio
<sup>63</sup> Cu	Copper Isotope
<sup>137</sup> Cs	Cesium Isotope
D-T	Deuterium–Tritium source
ENDF60	Evaluated Nuclear Data File at 60 series
F1	Surface Current
F4	Track length estimate of cell flux

F5	Flux at a point of the detector
F8	Energy distribution of pulses created in a detector
Gamma Ray	Gamma rays are electromagnetic radiation with very high energy
He-3	Helium-3 isotope
Hydrogen Index	The ratio of hydrogen atoms concentration per unit volume
MCNP	Monte Carlo Neutron Particle transport code
MCNPX	Monte Carlo Neutron Particle eXtended
MCNP4C	Monte Carlo Neutron Particle version 4C
$M_{\text{H}}/M_{\text{water}}$	Weight Fraction of the hydrogen in the water
$M_{\text{O}}/M_{\text{CaCO}_3}$	Weight Fraction of the oxygen in the limestone
$M_{\text{O}}/M_{\text{water}}$	Weight Fraction of the oxygen in water
$^{54}\text{Mn}$	Manganese Isotope
$^{22}\text{Na}$	Sodium Isotope
NaI	Sodium Iodide
Neutron	Is part of the nucleus of all atoms except hydrogen atoms, has no electrical charge, has mass $1.675 \times 10^{-27}$ kg
NNTE	Neutron-Neutron Thermal Epithermal logging tool

P%	Porosity percent
PGNAA	Prompt Gamma ray Neutron Activation Analysis
<sup>239</sup> Pu-Be	Plutonium Isotopes –Beryllium Source
<sup>124</sup> Sb-Be	Antimony Isotopes -Beryllium Source
Si/Ca	Silicon/Calcium
VisEd	MCNP Visual Editor (MCNP Geometry Plot )
$\rho_{\text{tot}}$	Density of the formation (limestone) after a percentage from the porosity

## **Chapter 1: Introduction**

### **1.1 Overview**

The well logging is a technique of making petro physical measurements in the sub-surface earth formations through a drilled borehole to reach the characterization of both the physical and chemical properties of rocks and fluids. For instance the existence of some spaces in the rock can be a signature for storage of the petroleum. If the rock has openings, voids or spaces in which liquid and gas may be stored, it is said to be porous. For a given volume of rock, the ratio of the open space to the total volume of the rock is called porosity [1-3]. Neutron tools are the oldest logging instruments which used radioactive sources in determining the porosity. Nuclear logs are the most important techniques among various types of logging tools. There are many tools used in well logging. This investigation concentrates on two important tools:

- The Carbon/Oxygen tool which has the ability to detect the presence of carbon atoms in oil and oxygen atoms associated with water.
- The neutron porosity which uses neutron-counting measurements to detect the presence of hydrogen atoms.

The optimization in combining these two tools is expected to enhance the well logging activity as well as to make it more effective.

### **1.2 Prompt Gamma-Ray Neutron Activation Analysis**

Prompt Gamma-ray Neutron Activation Analysis (PGNAA) is used to determine the elements in the samples that depends on inelastic scattering and radioactive capture in neutron- nuclear interaction. This interaction emits gamma-ray

which indicates the presence of a certain amount of element in a sample [4]; for instance 4.43 MeV energy of gamma-ray is an indication of carbon atoms, but 6.13 MeV and 3.68 MeV are indications for the existence of oxygen atoms [3].

### **1.3 Well Logging Tools**

Three essential types of logging tools have been developed to collect data overtime, namely: electrical, acoustic, and nuclear logs. In this sub-section, we will show the performance/operation of each of these three logs.

First, in electrical logging, an electrical circuit is designed to measure the resistivity of a component. There are many types of electrical logs such as: electrode resistivity devices, induction logging, micro resistivity logs, and spontaneous logs.

Second, acoustic logs are widely used in a variety of applications. They work by transmitting sound waves through a medium having porosity, then detecting the transmitted pulses. For instance, a good example can be seen in cement bond logs.

Third, nuclear logs exploit the neutrons emitted from the source, then pass through the sample and consequently cause the neutron to lose energy. The end of this process exhibits either absorbing or reflecting the neutrons back to the detector.

As a matter of fact, there are several types of nuclear logging: (i) gamma-ray logs, (ii) spectral gamma-ray logs, (iii) density logging, (iv) pulsed-neutron-lifetime logs, (v) geochemical logs, (vi) neutron porosity logs, and (vii) carbon/oxygen logs. This thesis will focus on combining two tools only: C/O tool and thermal-neutron-porosity tool. The selection of these two tools has been considered carefully in order

to serve the objectives of this study. C/O tool, and neutron-porosity tool in MCNP design [5,6] are shown in Figure 1.

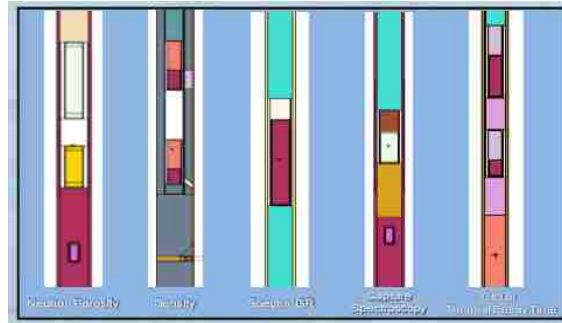


Figure 1: MCNP Design for Different Logging Tools [7]

### 1.3.1 Neutron-Porosity Logging Tool

Neutron-porosity-logging tool consists of one neutron source such as Am-Be, or D-T, or Cf-252, and two thermal neutron detectors such as He-3 detector, which responsible to detect on the neutrons. Some materials do have high capture cross section for thermal neutrons such as chlorine.

### 1.3.2 C/O Logging Tool

Carbon/ Oxygen tool, also called pulsed neutron spectral (PNs), consists of D-T accelerator source with two sodium iodide (NaI) detectors that are detecting the gamma rays emitted from inelastic interaction of fast neutrons with carbon and oxygen. Then, the C/O ratio from the gamma rays emitted could be estimated [8].

### 1.4 Neutron Source

Different types of neutron sources are presented: nuclear reactors, isotopic sources and accelerators. Nuclear reactors mostly produce thermal neutrons,

whereas, isotopic sources produce neutrons from spontaneous fission (SF) such as  $^{252}\text{Cf}$ , ( $\alpha,n$ ) reaction such as  $^{241}\text{Am-Be}$  and ( $\gamma,n$ ) reaction such as  $^{124}\text{Sb-Be}$ . Accelerators source produce fast neutrons such as D-T reaction, the fast neutrons produced have an energy of about 14 Mev. Figure 2 describes sealed tube neutron generator, which consists of a hollow cylindrical anode surrounded in both sides by cathode plates, external magnetic produces a coaxial field and leads to ionize the deuterium and tritium gas, when it enters into the anode the ions are accelerated by the potential difference between the exit cathode and the accelerator electrode. Accelerator ions strike the target of deuterium and tritium, form the fusion and neutrons with energy 14 Mev are generated. The generator produces neutrons with almost monoenergetic energy of 14 MeV. Neutrons of this energy are more effective in promoting inelastic gamma rays that are of importance in the C/O tool. [9,10].

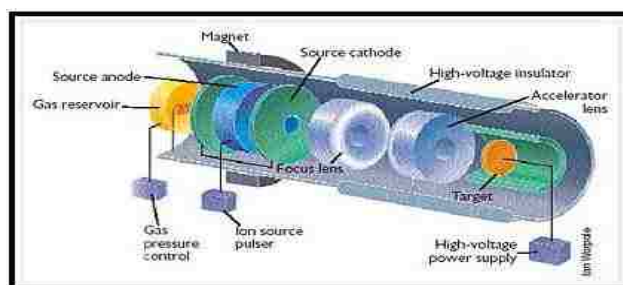


Figure 2: Sealed Tube Neutron Generator [10]

### 1.5 Well Logging Tool Detectors' Types

The previous section (Section 1.3) has shown that every tool should possess one or more detectors. Furthermore, there are many types of detectors to be used in well logging tool, for example: (i) gas filled detectors, (ii) semiconductor detectors, and (iii) scintillation detectors. Sodium iodide (NaI) has solid scintillation detector, which is used mostly to detect the gamma rays. NaI has high efficiency as well as it

is available in different sizes. It should be connected to a photomultiplier tube in order to amplify the scintillation light.

In the present study, NaI detector is crucially important, the next sub-section will be devoted to illustrate how it works. It is worth to mention that semiconductor-based detectors, such as those based on elementary semiconductors like Ge(Li) or Si(Li) or based on compound semiconductors like Cadmium-Telluride (CdTe), have better energy resolution than NaI detector [11] in detecting gamma-rays. Besides, there are other scintillation detectors which are also more efficient than NaI detector, such as: bismuth germinate (BGO) detector, Gadolinium Oxyorthosilicate (GSO), and lutetium oxyorthosilicate (LSO)[12]. Yet, traditionally NaI detectors have been broadly used more than any others.

### **1.5.1 Sodium Iodide Detector**

The Incident photons interact with the scintillation material atoms of NaI, which get excited and start emitting visible light on the photocathode. The absorption of this light by the photocathode results in the emission of photoelectrons which enter the photomultiplier tube. In the photomultiplier tube, the photoelectrons strike with the anode, causing a secondary electron to be emitted and get accelerated to reach the last electrode. This process produces pulses that get attracted to the anode and, subsequently, to the preamplifier. The preamplifier will produce amplified pulses with different amplitude depending on the original gamma-ray energy [13].



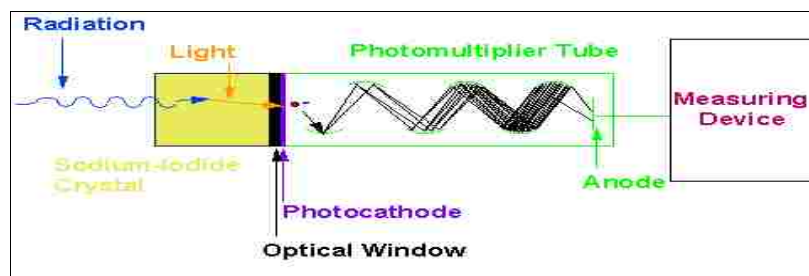


Figure 3: NaI Detector [14]

## 1.6 Statement of the Problem

This thesis investigates the optimization of the combined tool by studying different factors and assessing their effects on the tool response. These factors include: (1) lining thickness, (2) source-to-detector spacing, (3) borehole size and salinity, (4) temperature, (5) formation salinity, (6) capture cross section and (7) casing. We use the Monte Carlo N-particle (MCNP) package to examine the combined tool response to these factors. The preliminary results showed interesting facts. More specifically in this study, boron will be added to a NaI detector in order to combine both the carbon-oxygen (C/O) tool and the thermal-neutron-porosity tool into one tool (combined tool). It is expected that this optimized combined (C/O) and neutron-porosity-oil-well-logging tool to show efficient porosity sensitivity with a reduced incidence of neutrons on the detectors. As a result, the detector will be activated with least thermal neutrons. Also, it is anticipated that this tool reduces the cost of logging tools, simplifies the logging methods as well as reduces the time spent in obtaining well logging [15].

## 1.7 Introduction to Monte Carlo N-Particle Simulation

The Monte Carlo N-Particle (MCNP) package, originally developed in Los Alamos National Lab (USA), is a numerical algorithm to solve mathematical

problems based on the simulation of random variables. Monte Carlo method depends on the use of random numbers, probability and statistics to solve a certain specific problem. The main advantage of the Monte Carlo method is the short computer time needed to find solutions and the ability to provide approximate solutions to many realistic problems [16,17]. Concerning the MCNP in our present problem, the proposed combined tool is modeled using MCNP-transport code. Specific information is needed as input, such as those related to the tracing of fast neutrons, which were emitted from specific positions 33-cm away from the face of the near detector and passed through interaction with specific elements.

This is done by using the source specification SDEF card for the point source with a specific tally on a specific surface or volume of interest. F1 tally indicates to the incident thermal and epithermal neutrons on the specific surfaces of the near and far detectors; while F8 tally produces the energy distribution of pulses over a volume created in a detector. F8 tally indicates to the near detector count rate. F18 tally segment indicates to the far detector count rate, using 150 million to 250 million starting source neutron particles, within about seven to thirteen hours running time.

## **1.8 Relevant Literature**

Production-well-logging techniques provide information necessary for efficient and economical well performance. Many countries have provided considerable budgets to establish the RDUs (research and development units) to undertake a serious research in this field. We will illustrate the experiences of many countries outside UAE.

It is noticed that many researchers have extensively used MCNP simulation in many countries to investigate, for instance, the distance between source and detectors, and then the effect on the porosity sensitivity [18]. Authors of reference [18] used MCNP for the optimization of a neutron porosity probe design, and compared it with the experimental results. They reported that the probe became more sensitive to porosity resolution at a source-detector distance of more than 40cm. Their results showed a good agreement between the experimental results and simulation MCNP calculations. They used one million starting source particles, and about 9 minutes running time, and using F4, F5 tallies to measure the total number of the reaction in the detector, and obtained good estimates of the total flux over a surface. In this thesis, 150 million particles were used together with F1 and F8 tallies, and about 500 minutes running time. Another related work, Drabina and coworkers [19] studied the correlation between measurements and Monte Carlo simulation for Neutron-Neutron Thermal and Epithermal (NNTE) logging tool response. This is designed to measure the thermal neutron absorption, which contains Am-Be neutron source in three detectors. The near detector is used to measure thermal neutrons, while the other detectors are used to measure epithermal neutrons. The results showed good agreement between simulation and experiment and demonstrated that Boron to be an efficient absorbent of thermal neutrons.

In 2013, N.M. Chikhradze et al. [20] performed theoretical calculations, they used low-energy neutron in the range [1 eV – 10 eV] to show that the boron-based composites have better absorption performance, and have very large neutron absorption cross section. J. Liu and co-workers [21] used the MCNP simulation to study the effect of boron lining, inside and outside the pulsed neutron gamma element logging tool, on the counting rate of the gamma ray emissions. They have

concluded that boron lined outside the tool can reduce neutron damage to the detectors by decreasing the thermal neutron count. They reported that it is better in identifying the elements to use boron lined inside the tool. Then, they also studied the effects of borehole size and formation porosity on the porosity response. As results, they noticed that more than 10% of the porosity sensitivity increased because of the increased formation in water salinity; whereas the borehole size has a large impact on the porosity response.

Similarly, the work of W.A. Metwally [22], boron lined NaI detectors are used instead of He-3 detectors to avoid the latter detector's high cost. He found that boron-lined NaI detectors have a good sensitivity to neutrons at different source positions. The response of the boron-lined NaI detector is much higher than that of the He-3. To contrast between He-3 and B-10, in 2010 IEEE [23] compared the efficiency of neutron detection between He-3 counter and B-10 filled liquid scintillator. They found that the B-10 loaded liquid scintillator yield higher efficiency detection. Unfortunately, gamma-ray sensitivity remains high, and they tried to reduce the undesired gamma-ray sensitivity of the liquid scintillator through several attempts.

M. Shahriariband and M. Sohrabpour [24] used MCNP simulation in borehole surrounded by a granite formation with (Am-Be) neutron source. They studied the effect of the moisture on the thermal neutron. They correlated the increase in thermal neutrons with the increase in hydrogen atoms. The presence of materials, such as boron, cadmium, samarium, and gadolinium, etc, reduced the thermal neutron. With regard to the effect of the geometrical design, F. Li et al. [25] used MCNP in pulsed neutron as one of the nuclear logging tool to study the

distribution of the neutrons in the borehole and formation to track each neutron from its birth to its end. They calculated the neutrons property as function of energy, position. Indeed, those distributions could help the scientists to reach the best tool designs optimization. S. Korotkin et al. [26] used MCNP transport code to optimize a neutron detector using the He-3 based detector surrounded polypropylene. This would lead to the increase in its sensitivity for thermal neutron with different geometrical moderator configurations. They concluded that the rectangular box and elliptical shell, with reducing mass were optimal. In 2001, E. Akaho et al. [27] used thermal neutron reflection to determine the hydrogen in petroleum products in Ghana. This was done using an instrument composed of  $^{241}\text{Am}$ -Be neutron source and He-3 neutron detector. They used two different configurations of source sample geometries with different thicknesses placed in a cylindrical aluminum container of diameter 10 cm and height 10.4 cm. In the second trial, they used 9.7 cm in diameter and 100 cm in height. They concluded that the detection of thermal neutrons is sensitive to the geometrical arrangement and the thicknesses of moderators.

To investigate the effect of the type of the source on the tool response, in 2011, J.G. Fantidis et al. [28] used MCNPX in a comparative study of the performance of the prompt gamma ray neutron activation analysis (PGNAA) by using four different neutron sources:  $^{241}\text{Am}$ -Be ,  $^{252}\text{Cf}$  ,  $^{241}\text{Am}$ -B, and D-T. The prompt gamma ray neutron activation analysis was found to be at its best performance with  $^{252}\text{Cf}$  neutron source. From studying the effect of the neutron source on the porosity, C. R. Peebles et al [29] replaced the Am-Be neutron sources in neutron porosity logging tool by accelerator neutron sources as Deuterium-Tritium through MCNP5. Although D-T source is still be considered hazardous but controllable substance, they used Monte Carlo neutron transport simulation to

determine the alternatives for Am-Be sources, which differs in source neutron energies. Hence, this resulted in differences in the tool responses because the D-T fusion reaction produces neutrons with energy of 14 MeV, while  $^{252}\text{Cf}$  emit neutrons with energy of 2.1 MeV, and D-D fusion reaction emit neutrons with energy of 2.2 MeV. Although the performance of each source depends on the count rate uncertainty, the D-T accelerator source has the worst sensitivity of the response to porosity.

In 2012 A. Chen et al. [30] compared three neutron source (D-T, D-D, and Am-Be) in terms of their sensitivities to the formation porosity. The results showed that the D-D source have greater sensitivity than the other sources. The D-T neutron source has the lowest sensitivity. Recently, J. Liu et al. [31] published a paper about to report that the use of D-T neutron source in porosity logging tool instead of Am-Be source would improve the sensitivity of neutron porosity measurement to the formation porosity variation. The reason for this is that the D-T source is safer. Although with Am-Be source being sensitive to the formation porosity variation, it has less energy neutron emitted of about 4.5 MeV while D-T source has 14 MeV energy neutron emitted. With the increasing of neutron energy the interaction probability with hydrogen decreases, then it also reduces the ratio of the sensitivity to the porosity variation. They used MCNP simulation to study the response of neutron logging tool to hydrogen index and formation density. They achieved the porosity tool based on D-T source which was sensitive to small values of porosity but after density correction the tool became more sensitive to broader variation of porosity.

W.A. Metwally [15], used MCNP transport code and showed that D-T source have less sensitivity response to the porosity. Also in 2002 H. R. V. Carrillo et

al. [32] measured neutron and gamma-ray spectra for both  $^{239}\text{PuBe}$  and  $^{241}\text{Am-Be}$  sources, they noticed that the count rates of the 4.4 MeV gamma rays in both neutron sources produced the same photon strength per unit of the source activity. The effect of the distances between the source and the detector on the porosity, M. Rasoulinejad [33] attempted to reproduce the results of W.A. Metwally [15] via both simulation and experiment, Figure 6 in M. Rasoulinejad [33] paper shows the normalized ratio of the near to far detector counts versus formation porosity agree quite nicely especially at low porosity range between [0%-40%]. Although he used  $^{241}\text{Am-Be}$  isotopic source differently than in this latter paper (which used D-T neutron source) and with different spacing between source and detector, Metwally used at 33 cm while the author [33] used a 85 cm which led to different count numbers at every porosity value. Nevertheless, they agree that for small values of porosity, the tool is more sensitive to the formation porosity.

In 2013 W. Wu et al. [34] used theoretical calculations to study the effects of the distance between the source and the near detector, and the distance between the two detectors, on the porosity sensitivity. The results showed the porosity sensitivity to be highly sensitive at low values of porosity until 5% and then become almost constant at higher values of porosity. When increasing the distance between two detectors the sensitivity increases in the whole range of the formation. According to L. M. Scallan [35], the efficiency of five neutron detectors were compared by MCNPX modeling. L. M. Scallan [35] concentrated on the effect of moisture in the ground formation and the source detector distance on the count rate of the detectors. They found that the count rate decreases with increasing source detector distance. Although the count rate is affected by changes in ground composition only for simple

detectors, it is not affected by complex detectors, which have enough shields to prevent the detection of thermal neutrons.

In this work, NaI detector shielded with boron is used to study the effect of variation of source-detector distance on the counting rate. In the same contest, I. Akkurt et al. [36] studied the effect of the energy source and the distance from the source to the detector on the efficiency of the NaI (TI) detector using radioactive sources:  $^{22}\text{Na}$ ,  $^{54}\text{Mn}$ ,  $^{60}\text{Co}$ , and  $^{137}\text{Cs}$  to produce gamma ray at six different energies. For five different distances from the detectors, they found the efficiency of the detector to decrease with the increasing distance due to the increasing the source energy. D. Igwei [37] used MCNP simulation to study the effect of distance between neutron source and shielding materials (pure polythene and borated polythene) and thickness of shielding materials on the neutron dose. He found that for both shielding materials, the neutron dose decreases with the raise of shielding thickness and neutron source detector distance. The results also showed that the borated polythene had better shielding material than pure polythene. M. Basturk et al. [38] studied the neutron attenuation in boron mixture of stainless steel with a focus on the absorber content and material thickness to achieve the aimed beam attenuation. It was shown that thick samples using B-10 would strongly affect the neutron attenuation.

A. Shahri et al. [39] used MCNP4C to study the influence of lining thickness on the detector response. From their MCNP4C simulations and experimental results, the optimum lining thickness of boron lining appeared to be about 2 mm.

In this investigation, water is used in the borehole as a moderator; whereas J. Sun and P.Gardner [40] used  $^{124}\text{Sb}$ -Be neutron source to compare between MCNP



simulation and the experiment. They concluded that the water moderation is better in sensitivity than paraffin.

Prompt Gamma ray Neutron Activation Analysis (PGNAA) was used to determine the composition in the samples. For instance, in 1998, R. Khelifi et al. [41] performed PGNAA using Am-Be neutron source to analysis bulk concrete sample and they succeeded to determine the concentration ratio of Ca/Si based on the gamma-ray spectrum. On the other hand, in 2015, W. Jia et al.,[42] performed PGNAA to determine the type and amount of Boron and Cadmium dissolved in water, they found that PGNAA is very sensitive to the B and Cd because of their large neutron absorption cross section. In addition in 2016, F. Al-Shehri et al. [43] performed PGNAA to determine the elemental composition of a coal sample, which contains chlorine and sulfur. Also, M. Borsaru et al. [44] performed PGNAA to determine chlorine using  $^{252}\text{Cf}$  neutron source and BGO detector, which was surrounded by B-10. The polyethylene was placed in front of the detector, which was 60 mm away from the source. They found that the gamma rays energies related to the Cl element were: 6.1, 6.6, 7.4, and 7.8 MeV. Concerning cross section, T. Cywicka-Jakiel [45] used two kinds of data libraries (ENDF60 and ACTIA) for radioactive capture in Cl to study the influence of Cl in the borehole on the tool response. In the determination of the accuracy of the elements Si, Ca, and Fe, the results proved that the production in ACTIA library had more photons from radiation capture in Cl than ENDF60 does, and it also improved the accuracy of Si, Ca, and Fe elements determination. D. Igwes and O. Thomas [46] studied neutron macroscopic cross section and mean free path for polythene and borated polythene shields at different shield thickness and different distances between the source and detector using MCNP simulation. The results showed neutron macroscopic cross section and mean free

path to depend on the thickness of the shielding and on the distance between source and detector.

Another study concerning the optimization of well logging tool sensitivity, in 1997, H. Qing-Yuan et al. [47] investigated the improvement of the sensitivity chlorine spectrum logging tool, where the improvement tool consists of Am-Be source, and two detectors, with the near detector to be (He-3). They measured epithermal neutron, taking the far detector to be BGO, and measured gamma rays captured by chlorine instead of NaI detector. They reported that BGO to have more efficiency than NaI detector. The results gave evidence that the new tool to have more sensitivity. In 1990, M. Oraby et al. [48 ] performed MCNP to improve porosity sensitivity by proposed tool, which consists of  $^{241}\text{Am-Be}$  neutron source and two detectors. The (He-3) detector was near to the source and measured thermal neutrons, whereas the (NaI) detector is far from the source and measured prompt gamma rays. The results show that the proposed tool have more porosity sensitivity, and can reduce formation and borehole salinity dependence if compared with the conventional tool, which consists of the same neutron source and two thermal neutron near and far detectors (He-3).

## **1.9 Conception**

In this work, boron lining was added to the C/O logging tool, with the aim of combining both the C/O tool and the thermal-neutron porosity tool in one tool (combined tool). MCNP simulation was used to study the sensitivity of the combined tool to different values of porosity, especially low porosity region. The effect of the porosity sensitivity at different factors, which are: neutron cross section, formation

salinity, borehole salinity, lining thickness, source to detector spacing, borehole size, casing, and temperature. The rest of the thesis is composed as follows: Chapter 2 describes the methodology of the process; Chapter 3 shows the results; in Chapter 4 we discuss the results, and Chapter 5 presents a summary of the findings and the conclusions.

## Chapter 2: Methods

### 2.1 Combined Tool Design

Combined tool consists of C/O logging tool with an added Boron-10 lining with 0.2cm thickness film deposited on the two NaI detectors (near and far). The near detector is cylindrical in shape with 1.27-cm radius and 10.16-cm length, whereas the far detector is cylindrical in shape with 1.27-cm radius and 15.24-cm length. The spacing between center to center of the two detectors is 28 cm. The D-T neutron source position is at 33cm below the near detector. This source is responsible to emit fast neutrons of energy 14 MeV. The boron-lined detectors are placed outer of an aluminum casing of cylindrical shape with 0.05-cm thickness and 1.32-cm radius, with a copper cylinder of 1.27-cm length and 1.52-cm radius as windows detector. As a moderator material, we use a stainless steel cylinder of 2.143-cm radius and 250-cm length. The borehole is 4 inch in radius and filled with water. The formation consists of limestone ( $\text{CaCO}_3$ ) with pores, of various sizes, filled with water, as shown in Figure 4[15].

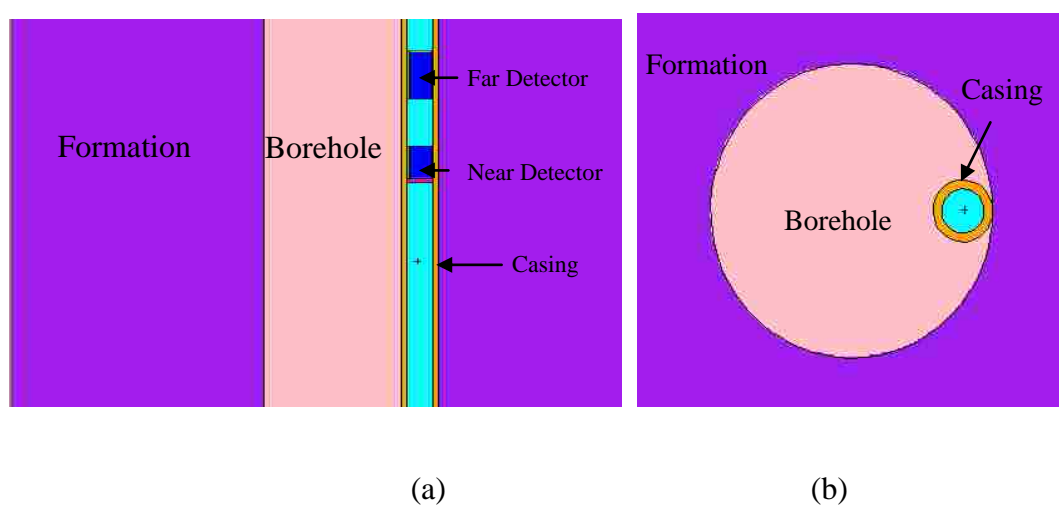
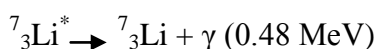
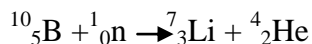


Figure 4: Monte Carlo Model of the Neutron-Porosity Tool with (a) an  $x$ - $z$  view and (b) an  $x$ - $y$  view

## 2.2 Thermal Neutron Interaction with Boron

We consider the following interaction equations [49]:



In MCNP simulation, we consider fast neutron emitted from D-T source with an approximate energy of 14 MeV. After many interactions of fast neutron with the formation atoms, the neutron loses energy until it reaches low values and becomes the so-called a “thermal neutron”. Thermal neutrons interact with boron as in the equation above, resulting in excited lithium nucleus which de-excites to the ground state by emitting 0.48-MeV gamma rays. Counting the number of 0.48-MeV gamma rays, should be a signature to indicate the formation of porosity. This number is proportional to the hydrogen atoms concentration. Figure 5 shows the neutron’s energy versus time to display the thermalization process of cooling fast neutron towards the state of thermal ones. The process takes time at order of ms.

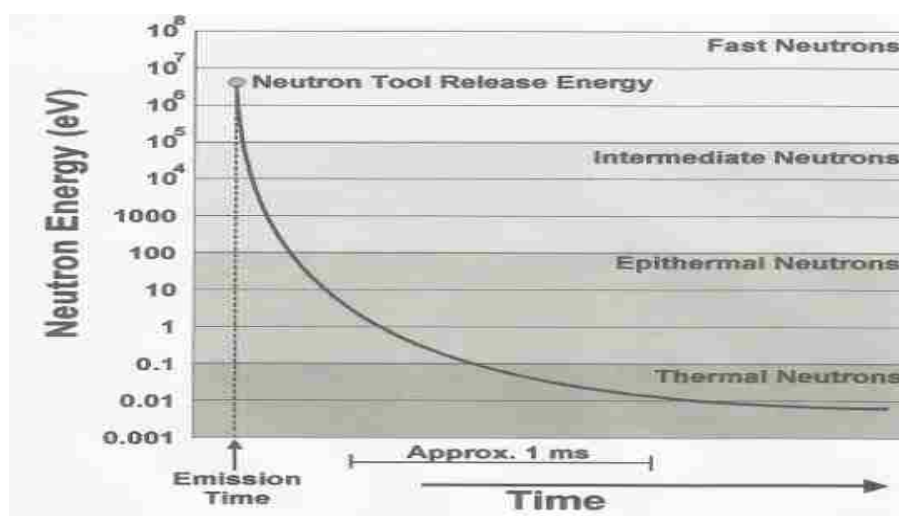


Figure 5: Neutron’s Energy Versus Time [50]

### **2.3 The Effect of the Source-to-Detector Spacing on the Combined Tool Response**

In order to change the neutron source position for the near detector different values are considered (15cm, 20cm, 25cm, 30cm, 35cm, 40 cm). MCNP is used to examine how these values will affect the combined-tool response. It should be emphasized that the increase of the distance traveled by the neutrons would expose them to more elastic and inelastic scattering and would increase their cross sections with atoms in the formation and in the borehole.

### **2.4 The Effect of Casing (Stainless Steel) Thickness on the Combined Tool Response**

Another factor to be tested is the change of stainless-steel thickness to the values (0.423cm, 0.473cm, 0.523cm, 0.573cm, 0.623cm), added one-by-one to the different values of the porosity. Stainless steel works as a moderator to reduce the number of incident neutron on the boron lining. This function is plausible because steel has a high average atomic number and a high density, which can cause a high attenuation to the gamma rays. Of course, this fact leads to a reduction in the photons count rate.

### **2.5 The Effect of the Borehole Size on the Combined Tool Response**

Borehole size effect depends on the borehole fluid. Borehole are usually filled with water. In this thesis, we need to change the size of the borehole using a set of values (5in, 6in, 7in, 8in, 9in, 10in) to study the effect of the borehole size on the combined tool response. We quote that increasing the size of the borehole would lead to an increase in the size of the water moderator. The borehole water can affect the

neutron transport because it contains the hydrogen atoms which have a significant effect on the count rate. Furthermore, neutrons are expected to slow down and reduce their energies to within the thermal energy range, as they interact with water.

## **2.6 The Effect of the Temperature on the Combined Tool Response**

In MCNP equation 1 is used to calculate the temperature of the cells [51]:

$$kT(\text{MeV}) = 8.617 \times 10^{-11}(T + 273.15) \quad (1)$$

where T is the temperature in degrees Celsius ( $^{\circ}\text{C}$ ), and the unit used in MCNP for kT is MeV.

The effect of the temperature is only due to the elastic scattering cross section. The values of T is considered as (0  $^{\circ}\text{C}$ , 10  $^{\circ}\text{C}$ , 20  $^{\circ}\text{C}$ , 30  $^{\circ}\text{C}$ , 40  $^{\circ}\text{C}$ , 50  $^{\circ}\text{C}$ ), to be used in studying its effects on combined-tool response. In MCNP, temperature is expected to have an effect only on the speed of the targets. It turned out that these small values of temperature have insignificant effects.

## **2.7 The Effect of the Cross Section on the Combined Tool Response**

In this section 60c and 70c series are used, and both are derived from cross section data from Evaluated Nuclear Data File (ENDF) / B-IV source. This has been done in order to study the effect of cross section on the combined tool response versus the porosity.

In the MCNP code simulation, the neutron, produced by the D-T source, move through the formation material toward the NaI detector. We assume that the neutron is transmitted through a material of thickness x and will undergo interactions as it moves through an absorber by either absorption or scattering cross section. For

example, let's suppose having a mono-energetic beam of neutron transmit some of initial intensity ( $I_0$ ) through the material (absorber) of thickness  $x$  and exit with intensity ( $I_x$ ) as shown in Figure 6. The ratio of the intensities is given by equation (2)[52]:

$$I_x/I_0 = \exp(-\Sigma x) \quad (2)$$

where:  $\Sigma$  stands for the total macroscopic neutron cross section;

$\exp(-\Sigma x)$ : is the “ Probability that the neutron will travel distance  $x$  without an interaction”[9]

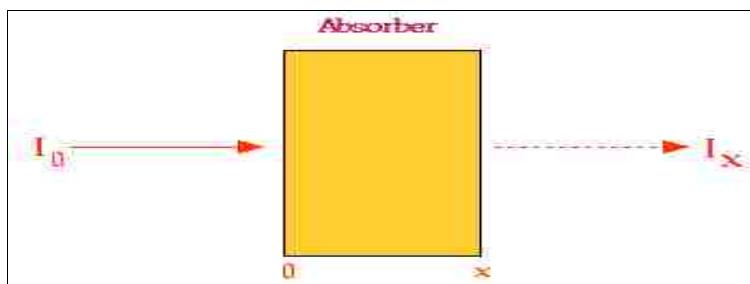


Figure 6: Neutron Beam Transmitted through the Absorber [52]

Comparing the previous equation number (2) with equation number (3) below

$$I_x/I_0 = \exp(-\mu x) \quad (3)$$

There exists a similarity between gamma attenuation coefficient ( $\mu$ ) and neutron macroscopic cross section ( $\Sigma$ ).



### **2.7.1 Attenuation of Gamma-Rays**

The total attenuation coefficient is the probability of interaction of a photon with a medium per unit length along the path. Factors affecting the attenuation of gamma rays:

- i. Atomic number of the medium (i.e., the larger the atomic number is the larger the attenuation should be).
- ii. Density of the medium (i.e., the lower the density of the absorber is the lower the attenuation should be).
- iii. Thickness of the medium (i.e., the thicker the absorber is the larger the attenuation should be).
- iv. Gamma-ray energy (i.e., the greater energy of the gamma rays is the lower the attenuation should be) [52].

### **2.7.2 Types of Neutron Interactions with Matter**

#### **2.7.2.1 Scattering**

In the scattering process, a neutron alters an interaction with nuclei of the matter, and both particles will appear after scattering. There are two ways for neutron scattering in the formation [9]:

##### **2.7.2.1.1 Elastic Neutron Scattering**

Elastic Scattering, where the neutron interacts with the nuclei without exciting it but the neutron loses energy (i.e., there is conservation of total linear momentum and conservation of total energy, but if we assume that the nuclei is at rest before the collision then one should expect a reduction of kinetic energy of

neutron after the collision) . For example, hydrogen is very good for slowing down neutrons because the mass of its nucleus is almost equal to that of neutron. Hence, if a formation slows down neutrons that should likely indicate the abundance of hydrogen.

#### **2.7.2.1.2 Inelastic Neutron Scattering**

In this process, neutron collides with the nuclei and part of the neutron kinetic energy is given to the nuclei as excitation energy. Then, the excited nuclei will return to the ground state by emitting gamma rays. C/O logging can measure the gamma rays emitted during the inelastic neutron scattering to determine relative concentrations of carbon and oxygen in the formation [9].

#### **2.7.2.2 Absorption**

In absorption interaction, the neutron disappears completely, and other particle is produced and will appear after the scattering event [9].

#### **2.7.3 Neutron Cross Section [ $\sigma(\text{m}^2)$ ]**

Neutron cross section is defined to be: "the probability that an interaction will occur per target nucleus per neutron per  $\text{m}^2$  in hitting the target", it has (barns) unit also. Neutron cross section depends on:

- 1- The energy of the neutron.
- 2- The mass number of the target nucleus [9].

### **2.7.4 Macroscopic Cross Section [ $\Sigma$ ( $\text{m}^{-1}$ ) ]**

This is defined to be: "the probability that any interaction type will take place per unit distance of travel of a neutron moving in a medium that has a density of nuclei/ $\text{m}^3$ " [9].

### **2.7.5 Mean Free Path [ $\lambda(\text{m})$ ]**

Mean free path is defined to be: "the average distance between two consecutive interactions". Also it is defined as the inverse of the total linear attenuation coefficient ( $1/\mu$ ), or as the inverse of the macroscopic cross section ( $1/\Sigma$ ) [9].

## **2.8 The Effect of the Borehole Salinity on the Combined Tool Response**

We consider replacing the water in the borehole by water of different percentages of salinity (i.e., 0%, 5%, 10%, 15%, 20%, 25%, 30%), then we use MCNP simulation to study the correlation between the salinity and combined tool response. Here, we clarify that chlorine is known to be a strong absorber of thermal neutrons (i.e., the more salinity percentage is the more neutrons absorbed in the borehole should be).

### **2.8.1 Calculation of Density and Weight Fraction**

The purpose here is to show how to calculate the density of saline water and the weight fraction of the elements contained in the borehole of different values porosity.

From the definition of salinity:

$$S = \frac{m(\text{NaCl})}{m(\text{sw})} \quad (4)$$

Where mass of saline water is:

$$m(\text{sw}) = m(\text{water}) + m(\text{NaCl}) \quad (5)$$

Substitute equation (5) into equation (4) yields

$$m(\text{NaCl}) = m(\text{water}) \frac{S}{1-S} \quad (6)$$

The volume of salt can be obtained from:

$$V(\text{NaCl}) = \frac{m(\text{NaCl})}{\rho(\text{NaCl})} \quad (7)$$

Where  $\rho(\text{NaCl})$  stands for the mass density of salt. The volume of water should be:

$$V(\text{water}) = V(\text{sw}) - V(\text{NaCl}) \quad (8)$$

After substitute equations (6,7) into equation (8), volume of water becomes

$$V(\text{water}) = \frac{m(\text{sw})}{\rho(\text{water})} - \frac{m(\text{sw}) S}{\rho(\text{NaCl})(1-S)} \quad (9)$$

We can calculate the volume of borehole by using cylindrical volume equation, which is related to the saline water volume  $V(\text{sw})$ , then it can be used to calculate the density of the borehole fluid ( $\rho_b$ ) from this equation number (10) below

$$\rho_b = \frac{m(\text{sw})}{V(\text{sw})} \quad (10)$$

Weight fraction for each element can be calculated using the same steps as illustrated in this example when calculate weight fraction for the hydrogen as follows:

First, calculate the weight of hydrogen element in the water by using equation number (11):

$$W_t(\text{H}) = \frac{N_i \cdot A_i}{M_i} \quad (11)$$

Then, calculate weight fraction for hydrogen by using equation number (12):

$$W_f(\text{H}) = \frac{W_t(\text{H})}{W_t(\text{H}) + W_t(\text{O})} \quad (12)$$

Where  $W_f$  is the weight fraction

$N_i$  : number of atoms of the  $i^{\text{th}}$  element in the compound

$A_i$  : atomic weight of the  $i^{\text{th}}$  element

$M_i$  : molecular weight of the  $i^{\text{th}}$  element

## 2.9 The Effect of the Formation Salinity on the Combined Tool Response

We consider the formation composed of  $\text{CaCO}_3$ , whose density is  $2.711\text{g/cm}^3$ . From the section 3.1, replace the pure water in the pores by saline water with different percentage of salinity as used in section 2.8, then calculate the density of formation and weight fraction for Ca, C, O, H, Na, and Cl at different values of porosity and salinity. From MCNP simulation results, one can study the effect of formation salinity on the combined tool response, after adding Na and Cl elements to the pores.

After calculating the volume of the formation ( $V_F$ ) as a volume of cylindrical, and the weight of the rock (limestone) ( $W_R$ ) by using equation (13), below, to calculate the volume of the rock, then multiply by the density of the rock ( $2.711\text{g/cm}^3$ ) to calculate  $W_R$ , one obtains:

$$V_R = (1-P) V_F \quad (13)$$

where P is the porosity

$$V_P = PV_F \quad (14)$$

Using equation (14) to calculate the volume of the porosity ( $V_P$ ) which is related to the volume of the saline water ( $V_{sw}$ ) then using equation number (9) to calculate the volume of pure water. The weight of the pure water, whose density is  $1.0\text{g/cm}^3$ , also using equation number (6) to calculate the weight of NaCl. Now, one can calculate the density of the formation by using equation number (15):

$$\rho_F = \frac{W_{NaCl} + W_{H_2O} + W_{Rock}}{V_{NaCl} + V_{H_2O} + V_{Rock}} \quad (15)$$

Weight fraction can be found for each element as it will be explained in section 2.8.1.

## 2.10 The Effect of the Boron Thickness on the Combined Tool Response

By changing the boron lining thickness at various values such as (0.05 cm, 0.10 cm, 0.15 cm, 0.20 cm, 0.25 cm, 0.30 cm, 0.35 cm), and taking the mean free path of thermal neutron absorption cross section in the boron to be 0.002 cm, MCNP simulation was used to study the effects of every thickness at specific porosity on the combined tool response. It is of common sense to say that increasing boron thickness would enhance the adsorption cross section of the thermal neutrons.

## 2.11 Calculation of the Sensitivity Ratio

Equation (16) is used to calculate the response function (so named sensitivity) which is shown in the sensitivity figures.

$$F = (\Delta R/R_1)*100= [(R_i-R_1)/R_1 ]*100 \tag{16}$$

Where:

F: Sensitivity Factor

R<sub>1</sub>: The count value at 0% of the porosity obtained from the normalized counts

R<sub>i</sub>: Count values at different values of the porosity from the normalized counts

### 2.11.1 Calculation of the Sensitivity Error

The sequence or series formula shown in equation (17) is used to derive the sensitivity ratio error as follows [53]:

$$\sigma_u^2 = \left(\frac{\partial u}{\partial x}\right)^2 \sigma_x^2 + \left(\frac{\partial u}{\partial y}\right)^2 \sigma_y^2 + \dots \tag{17}$$

Let's assume that:

$$u = F = \frac{R_i - R_1}{R_1} \quad \text{and in math language:} \quad u = \frac{y - x}{x}$$

with: y=R<sub>i</sub> and x=R<sub>1</sub>, then:

$$\frac{\partial u}{\partial x} = -\frac{y}{x^2} = -\frac{R_i}{R_1^2} \tag{17-a}$$

$$\frac{\partial u}{\partial y} = \frac{1}{x} = \frac{1}{R_1} \tag{17-b}$$

Substituting the expressions in (17-a) and (17-b) into equation (17) yields:

$$\sigma_u = \left[ \left(\frac{R_i}{R_1^2}\right)^2 \sigma_{R_1}^2 + \left(\frac{1}{R_1}\right)^2 \sigma_{R_i}^2 \right]^{1/2} \tag{18}$$

Where: σ<sub>u</sub> : Sensitivity error

σ<sub>R<sub>1</sub></sub>: The error value of the count value R<sub>1</sub>

σ<sub>R<sub>i</sub></sub>: The error value of the count value R<sub>i</sub>

## Chapter 3: Results

It is important to note that all the MCNP results in this chapter are normalized per source particle.

### 3.1 The Effect of Porosity on the Combined Tool Response

Based upon the MCNP output files, F8 and F18 tallies refer to the near and far detectors, respectively, which are responsible for detecting the number of photons that are emitted within the energy range [0.4585 MeV- 0.5365 MeV]. Information about the number of thermalized neutrons, which is in turn proportional to the number of hydrogen atoms existing in the pore, can be extracted. From such information one can extrapolate the porosity.

#### 3.1.1 The Effect of Porosity on the Limestone Density

Table 1 presents the parameters of limestone ( $\text{CaCO}_3$ ) formation density versus porosity.

Table 1: Variation of Limestone Density versus Porosity

Porosity (%)	$\text{CaCO}_3$ density ( $\text{g/cm}^3$ )
0	2.711
5	2.57545
10	2.4399
15	2.30435
20	2.1688
25	2.03325
30	1.8977
35	1.76215
40	1.6266
45	1.49105



With the increasing porosity, the Limestone density decreases.

### 3.1.2 Calculation of Weight Fraction for Formation Elements

The density of limestone and the weight fraction for Ca, C, O and H are calculated, for instance, at 5% of Porosity as follows:

We used equation (19) to calculate the density of the formation at a given porosity

$$\rho_{\text{tot}} = (1-P) \times \rho_{\text{CaCO}_3} \quad (19)$$

Where:  $\rho_{\text{tot}}$ : is the density of the formation (limestone) at a given porosity

$\rho_{\text{CaCO}_3}$ : is the density of the formation (limestone) at zero porosity

P: is the porosity percentage

Then, by substituting into equation (19) with 5% of porosity, one gets:

$$\rho_{\text{tot}} = (1-5\%) \times \rho_{\text{CaCO}_3} = (1-0.05) \times (2.711) = 2.57545 \text{ g/cm}^3$$

Then, one can calculate the weight fraction of calcium:

$$w_{\text{Ca}} = \left(1 - \frac{P}{100}\right) \times \frac{40}{100} = \left(1 - \frac{5}{100}\right) \times 0.400 = 0.3922$$

Then, one can calculate the weight fraction of carbon:

$$w_{\text{C}} = \left(1 - \frac{P}{100}\right) \times \frac{12}{100} = \left(1 - \frac{5}{100}\right) \times 0.120 = 0.1177$$

Then one calculates the weight fraction of oxygen:

$$w_{\text{O}} = \left(1 - \frac{P}{100}\right) \times \frac{48}{100} + \left(1 - \frac{P}{100}\right) \times \frac{16}{100} = \left(1 - \frac{5}{100}\right) \times 0.888 + \left(1 - \frac{5}{100}\right) \times 0.480$$

$$w_{\text{O}} = 0.4879$$

Also, one can calculate the weight fraction of hydrogen:

$$w_{\text{H}} = \left(1 - \frac{P}{100}\right) \times \frac{2}{100} = \left(1 - \frac{5}{100}\right) \times 0.112 = 0.0022$$

### 3.2 Calculation of Error

Now, we address the question of how to calculate the errors? The way to do that is using the general propagation of error as follows:

To calculate  $\delta_a$  and  $\delta_b$ , which represent the errors in near and far detectors, respectively, we use the following equation [54]:

$$\delta = [(A_1 \times B_1)^2 + (A_2 \times B_2)^2 + \dots]^{1/2} \quad (20)$$

Where: A is photons count at a given value of energy from within the planned energy range.

B is the relative error at a given value of energy versus to the photons count from within the same energy interval.

Example:

$$\begin{aligned} \delta_a &= [(7.30000E-06 \times 0.0302)^2 + (6.18000E-06 \times 0.0328)^2 + (1.04473E-04 \times 0.0080)^2 + \\ &(5.24667E-06 \times 0.0356)^2 + (4.96667E-06 \times 0.0366)^2 + (4.71333E-06 \times 0.0376)^2 + \\ &(1.77000E-05 \times 0.0194)^2 + (4.42667E-06 \times 0.0388)^2 + (3.84000E-06 \times 0.0417)^2]^{1/2} \\ &= 1.03E-06 \end{aligned}$$

Values were taken from the output file (F8 tally) at 0% of porosity, as shown below in Table 2:

Table 2: Output File of Near Detector Counts

<b>Photon energy (Mev)</b>	<b>counts/source particle</b>	<b>Error</b>
4.5854E-01	7.30000E-06	0.0302
4.6829E-01	6.18000E-06	0.0328
4.7805E-01	1.04473E-04	0.0080
4.8780E-01	5.24667E-06	0.0356
4.9756E-01	4.96667E-06	0.0366
5.0732E-01	4.71333E-06	0.0376
5.1707E-01	1.77000E-05	0.0194
5.2683E-01	4.42667E-06	0.0388
5.3659E-01	3.84000E-06	0.0417

Tables (3) and (4) show the errors at a given value of porosity, and a given value of count of photons. We got from the summation of the photon count at the photon energy range [0.4585 MeV, 0.5365 MeV] for near and far detectors, respectively.

Table 3: Near Detector Counts

<b>Porosity (%)</b>	<b>counts/source particle</b>	<b>Error</b>
0	1.59E-04	1.03E-06
5	1.38E-04	9.61E-07
10	1.28E-04	9.20E-07
15	1.21E-04	8.98E-07
20	1.15E-04	8.77E-07
25	1.13E-04	8.69E-07
30	1.11E-04	8.58E-07
35	1.05E-04	8.34E-07
40	1.01E-04	8.21E-07
45	1.01E-04	8.21E-07

Table 4: Far Detector Counts

<b>Porosity (%)</b>	<b>counts/source particle</b>	<b>Error</b>
0	3.66E-05	4.94E-07
5	2.52E-05	4.10E-07
10	2.18E-05	3.82E-07
15	1.95E-05	3.60E-07
20	1.77E-05	3.44E-07
25	1.73E-05	3.40E-07
30	1.69E-05	3.36E-07
35	1.68E-05	3.35E-07
40	1.67E-05	3.34E-07
45	1.63E-05	3.29E-07

Figures 7 and 8 show the count of photons versus porosity for both near and far detectors, respectively, which resulted from the neutrons that have been traveled through the formation.

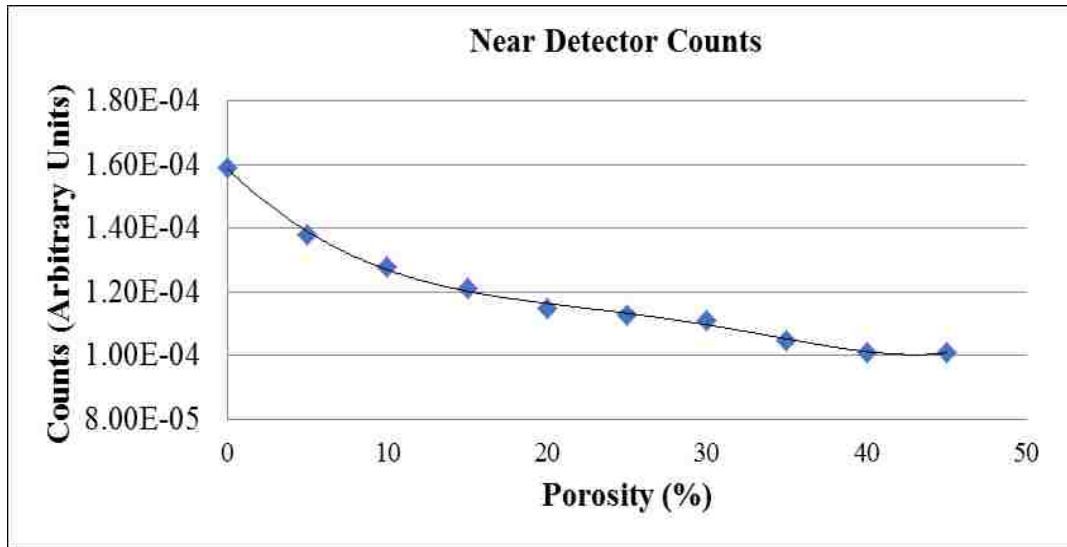


Figure 7: Near Detector Counts

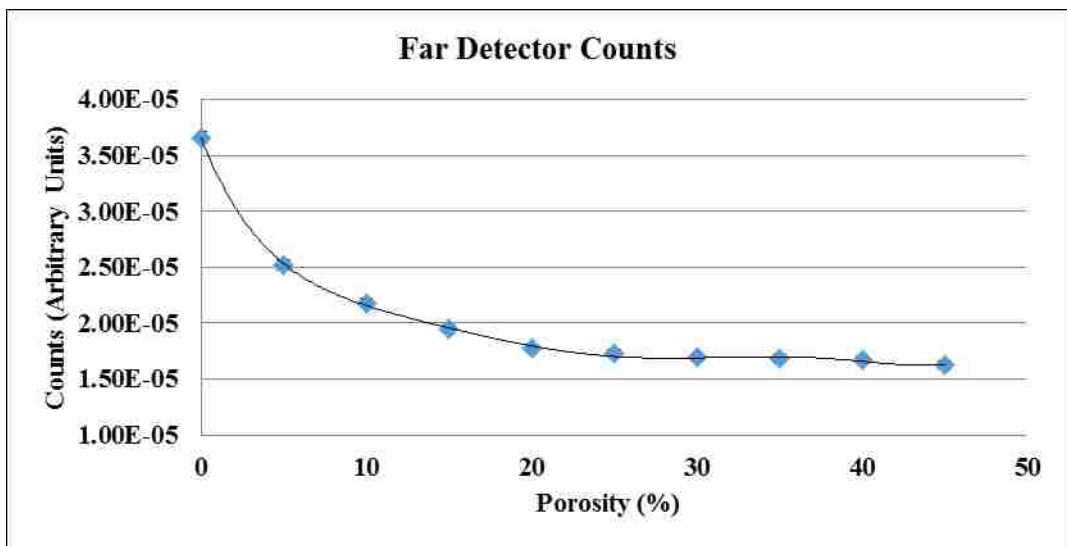


Figure 8: Far Detector Counts

Figure 9 shows the normalized ratio of near to far detectors counts versus porosity with errors.

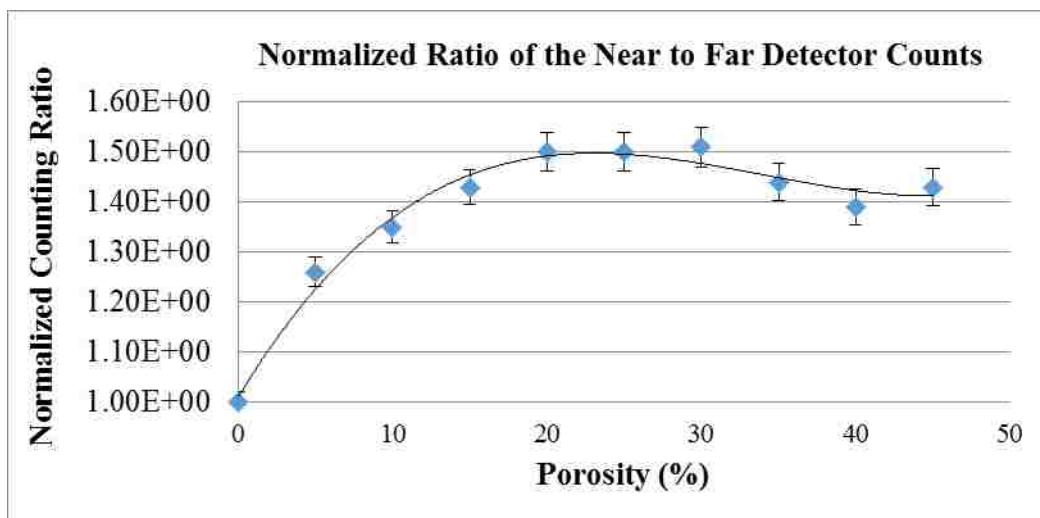


Figure 9: Normalized Ratio of the Near to Far Detector Counts

The steps, below, show how to calculate the normalized ratio, which is displayed in Figure 8:

First, we divide the near detector count on the far detector count at a given porosity as follows:

$$N_0/F_0 = 1.59E-04/3.66E-05=4.34E+00$$

$$N_5/F_5 = 1.38E-04/ 2.52E-05= 5.48E+00$$

$$N_{10}/F_{10} = 1.28E-04/ 2.18E-05= 5.87E+00$$

$$N_{15}/F_{15} = 1.21E-04/ 1.95E-05= 6.21E+00$$

$$N_{20}/F_{20}= 1.15E-04/ 1.77E-05= 6.50E+00$$

$$N_{25}/F_{25}= 1.13E-04/ 1.73E-05= 6.53E+00$$

$$N_{30}/F_{30}= 1.11E-04/ 1.69E-05= 6.57E+00$$

$$N_{35}/F_{35}= 1.05E-04/ 1.68E-05= 6.25E+00$$

$$N_{40}/F_{40}= 1.01E-04/ 1.67E-05= 6.05E+00$$

$$N_{45}/F_{45} = 1.01\text{E-}04 / 1.63\text{E-}05 = 6.20\text{E+}00$$

Then, we divide near to far detectors count at a given porosity on the near to far detectors count at zero porosity to get the normalized ratio as follows:

$$\frac{N_{45}(\phi=0.00)}{N_{45}(\phi=0.00)} = \frac{1.01\text{E-}04}{1.01\text{E-}04} = 1.00\text{E+}00$$

$$\frac{N_{45}(\phi=0.01)}{N_{45}(\phi=0.00)} = \frac{1.26\text{E-}04}{1.01\text{E-}04} = 1.26\text{E+}00$$

$$\frac{N_{45}(\phi=0.02)}{N_{45}(\phi=0.00)} = \frac{1.35\text{E-}04}{1.01\text{E-}04} = 1.35\text{E+}00$$

$$\frac{N_{45}(\phi=0.03)}{N_{45}(\phi=0.00)} = \frac{1.43\text{E-}04}{1.01\text{E-}04} = 1.43\text{E+}00$$

$$\frac{N_{45}(\phi=0.04)}{N_{45}(\phi=0.00)} = \frac{1.50\text{E-}04}{1.01\text{E-}04} = 1.50\text{E+}00$$

$$\frac{N_{45}(\phi=0.05)}{N_{45}(\phi=0.00)} = \frac{1.50\text{E-}04}{1.01\text{E-}04} = 1.50\text{E+}00$$

$$\frac{N_{45}(\phi=0.06)}{N_{45}(\phi=0.00)} = \frac{1.51\text{E-}04}{1.01\text{E-}04} = 1.51\text{E+}00$$

$$\frac{N_{45}(\phi=0.07)}{N_{45}(\phi=0.00)} = \frac{1.44\text{E-}04}{1.01\text{E-}04} = 1.44\text{E+}00$$

$$\frac{N_{45}(\phi=0.08)}{N_{45}(\phi=0.00)} = \frac{1.39\text{E-}04}{1.01\text{E-}04} = 1.39\text{E+}00$$

$$\frac{N_{45}(\phi=0.09)}{N_{45}(\phi=0.00)} = \frac{1.43\text{E-}04}{1.01\text{E-}04} = 1.43\text{E+}00$$

Table 5 below shows the values of the normalized ratio with errors versus porosity

Table 5: Normalized Ratio with Error versus Porosity

Porosity (%)	(N/F)/N0/F0	Errors
0	1.00E+00	0.021173
5	1.26E+00	0.029221
10	1.35E+00	0.03263
15	1.43E+00	0.035567
20	1.50E+00	0.038423
25	1.50E+00	0.038905
30	1.51E+00	0.039401
35	1.44E+00	0.03765
40	1.39E+00	0.036575
45	1.43E+00	0.037673

Here, the last step to calculate the errors in the normalized ratio by using equation

(21) [54]:

$$\delta(N/F) = [(1/b^2) \delta_a^2 + (a/b^2)^2 \delta_b^2]^{1/2} \quad (21)$$

Where a and b are near and far detectors count,  $\delta_a$  and  $\delta_b$  are errors corresponding to the counts in the near and far detectors, respectively.

Example: To calculate the error at 5% porosity for the normalized ratio:

$$\delta(N_0/F_0) = \left[ \frac{1}{(1.00E+00)^2} (0.021173)^2 + \left( \frac{1.26E+00}{(1.00E+00)^2} \right)^2 (0.021173)^2 \right]^{1/2} =$$

0.06503936



$$\delta(N_5/F_5) = \left[ \frac{1}{(2.729 \times 10^4)^2} \left( \frac{0.611 \times 10^4}{0.7} \right)^2 + \left( \frac{11.203 \times 10^4}{(2.729 \times 10^4)^2} \right)^2 \left( \frac{4.109 \times 10^4}{0.7} \right)^2 \right]^{1/2} =$$

0.096914926

We consider:  $\frac{11.203 \times 10^4}{(2.729 \times 10^4)^2} = 5.476190476$  as a,  $\frac{11.203 \times 10^4}{(2.729 \times 10^4)^2} = 4.344262295$  as b.

We use  $\delta(N_5/F_5)$  as  $\delta_a$ ,  $\delta(N_0/F_0)$  as  $\delta_b$ , then we use the same above equation (21) to get:

$$\delta\left(\frac{N_0/F_0}{N_5/F_5}\right) = \left[ \frac{1}{(2.729 \times 10^4)^2} \left( \frac{0.096914926}{0.7} \right)^2 + \left( \frac{4.344262295}{(2.729 \times 10^4)^2} \right)^2 \left( \frac{0.096914926}{0.7} \right)^2 \right]^{1/2} =$$

0.029221

### 3.3 The Reduction of the Neutron Flux Incident on the Detectors

One should use F1 tally in MCNP as an input file for obtaining the neutron current incident on the detectors, which in itself is an input file for MCNP F1:N6. That means that neutron current incident on the surface 6 which refers to detectors, and by using FS tally segment as is written in the input file FS1 -4 -5 -9 -10 to divide surface 6 into segments, where -4,-5 determine near detector surface, and -9,-10 determine far detector surface. The following Figures (10-15) display the neutron current incident on the near and far detectors with and without the boron lining in cases of thermal, epithermal, and fast neutron energy range, respectively. They actually demonstrate the effect of the boron lining on the detectors by reducing neutrons flux incident on the detectors.

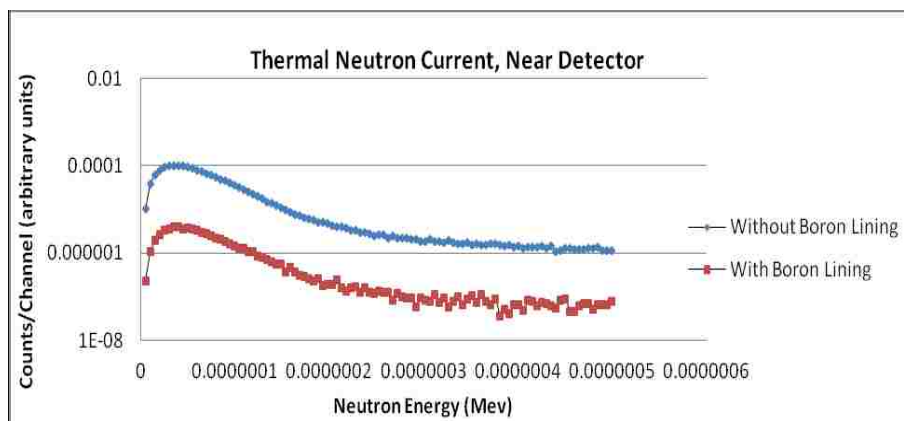


Figure 10: Neutron Current in the Near Detector, Thermal Energy Range

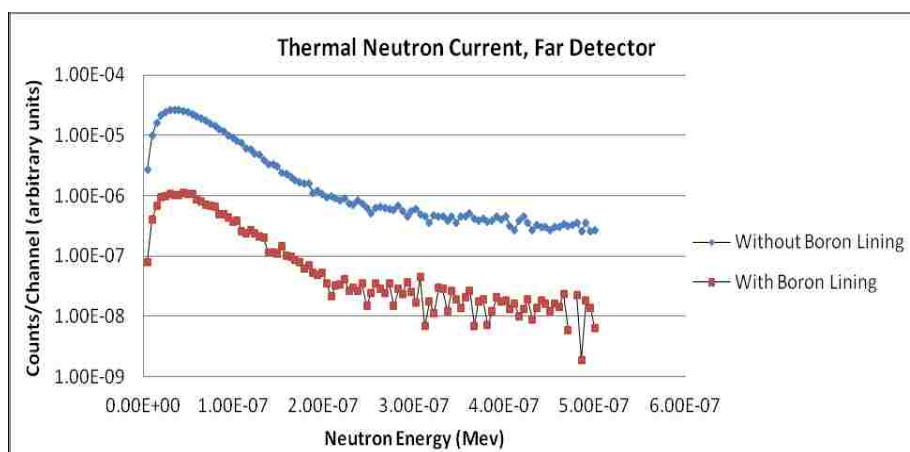


Figure 11: Neutron Current in the Far Detector, Thermal Energy Range

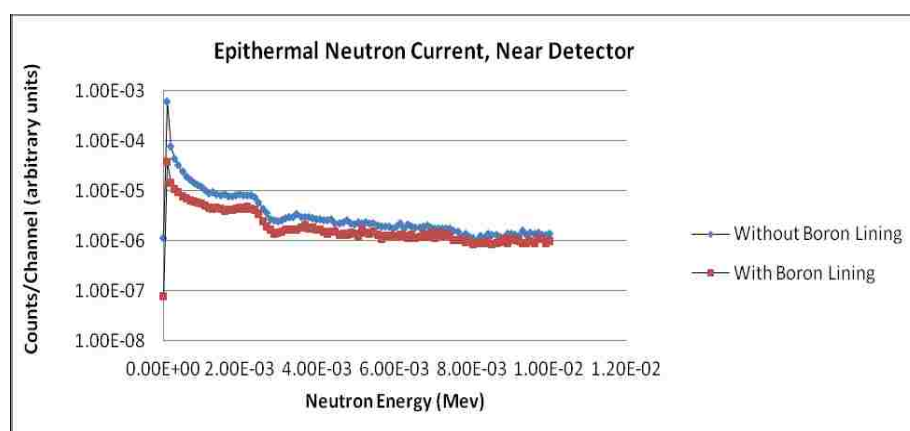


Figure 12: Neutron Current in the Near Detector, Epithermal Energy Range

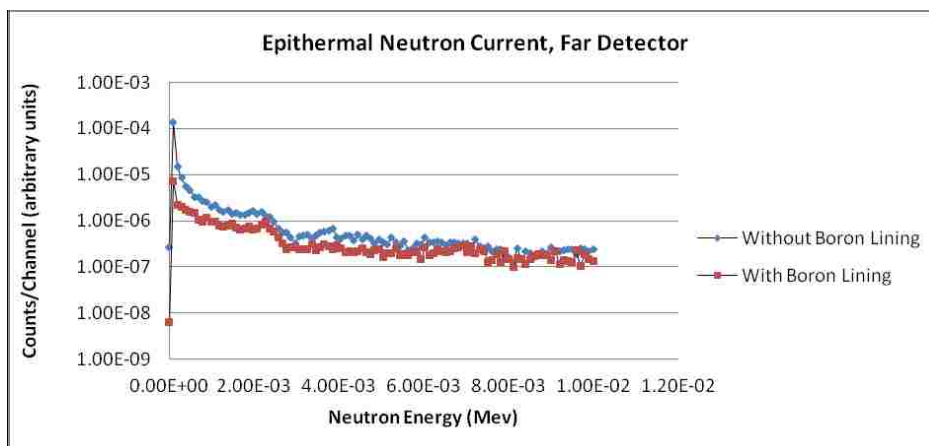


Figure 13: Neutron Current in the Far Detector, Epithermal Energy Range

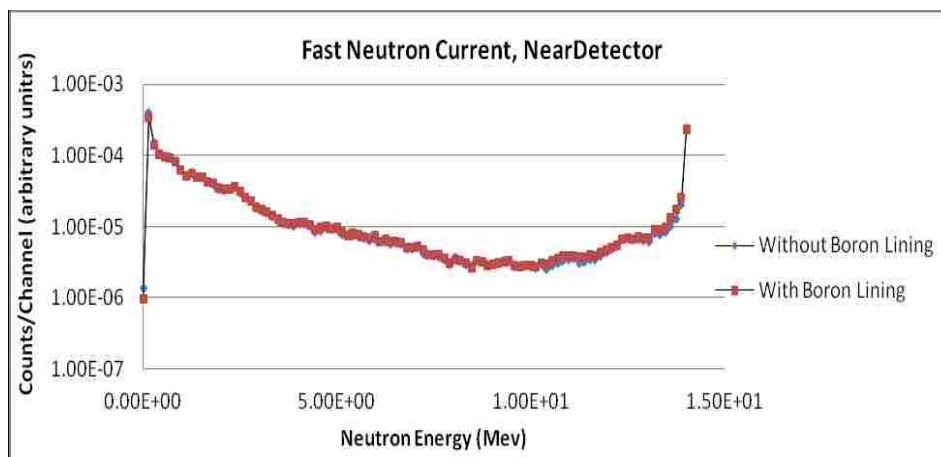


Figure 14: Neutron Current in the Near Detector, Fast Energy Range

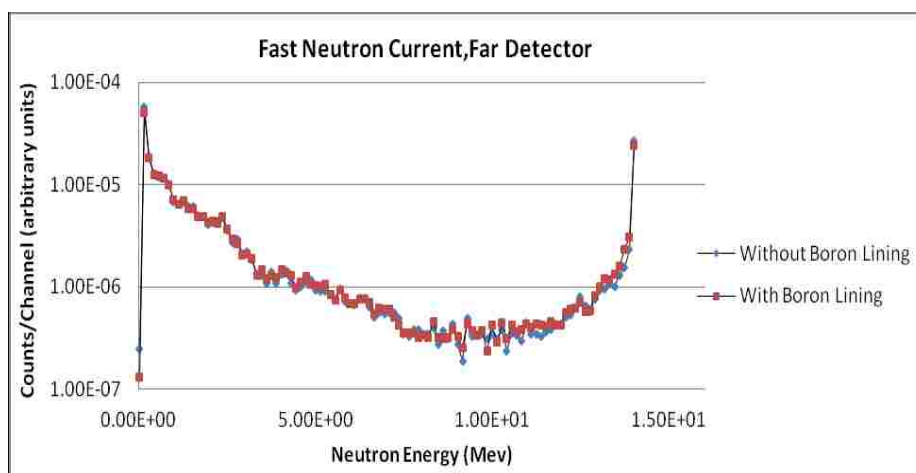


Figure 15: Neutron Current in the Far Detector, Fast Energy Range

### 3.4 Factors Affecting on the Combined Tool Response Results

#### 3.4.1 Source-to-Detector Spacing Results

At different distances from the source to the near detectors face at (15cm, 20cm, 25cm, 30cm, 35cm, and 40cm), figures 16 and 17 present the counts of photons as a function of porosity for both near and far detectors at different distances from the source to the face of the near detector.

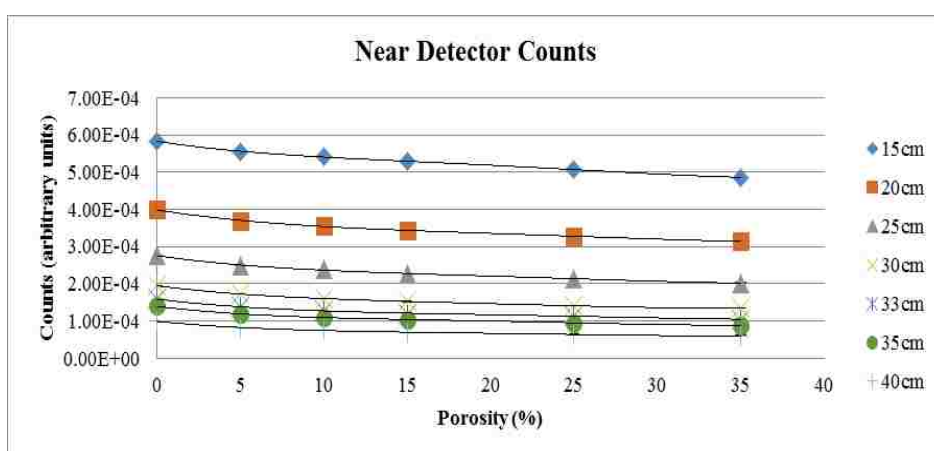


Figure 16: Counts versus Porosity and Source-to-Detector Distance, Near Detector

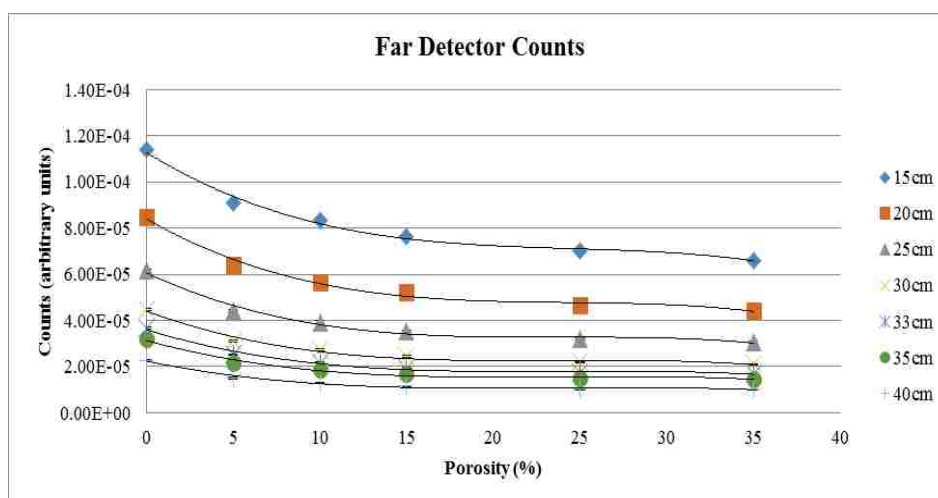


Figure 17: Counts versus Porosity and Source-to-Detector Distance, Far Detector

Figure 18 shows the normalized ratio versus porosity at different distances between the source and the face of near detector, while using the same procedure shown in section 3.2.

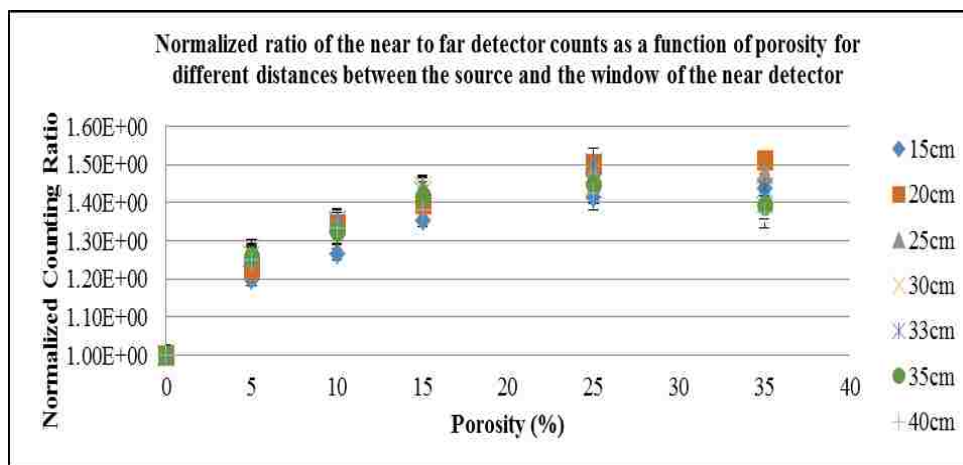


Figure 18: Normalized Ratio versus Porosity and Source-to-Near Detector Distance

### 3.4.2 Casing (Stainless Steel) Thickness Results

Figures 19 and 20 show the variation of photon count versus porosity when the moderator thickness of stainless steel is varied.

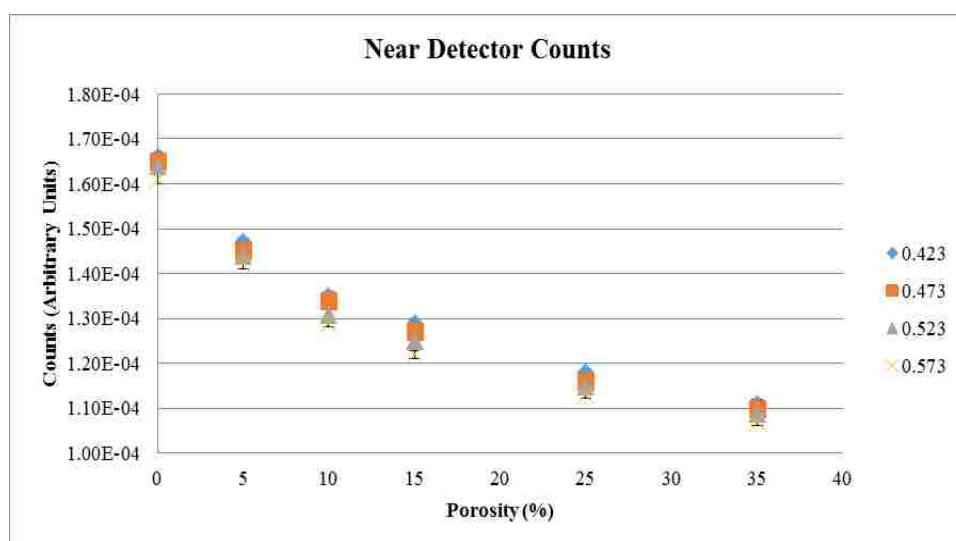


Figure 19: Count Rate versus Porosity and Casing-Thickness, Near Detector

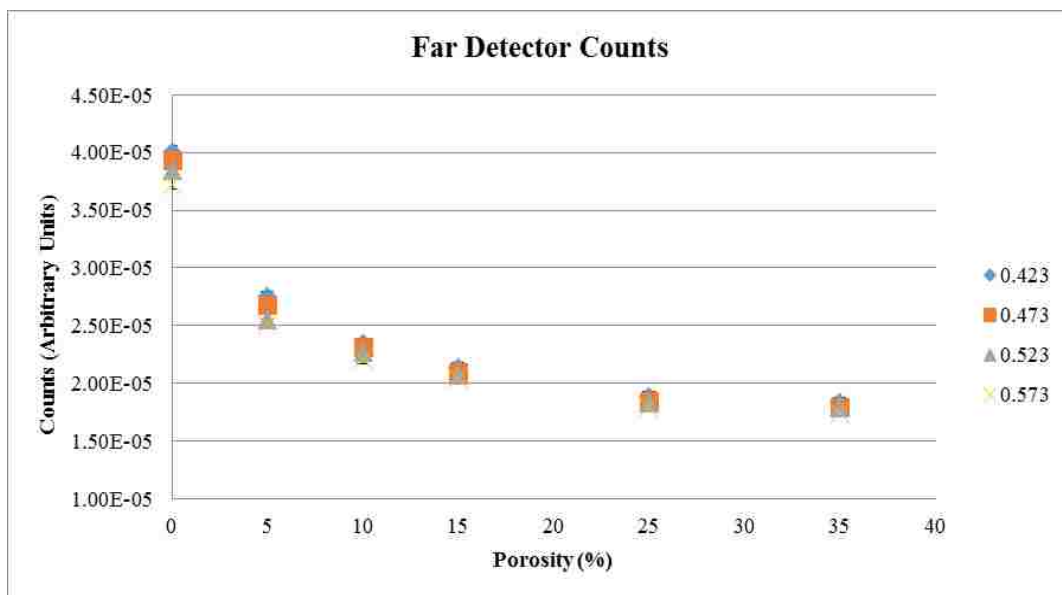


Figure 20: Count Rate versus Porosity and Casing-Thickness, Far Detector

Figure 21 shows normalized ratio versus porosity for the near to far detectors with different stainless steel (casing) thickness.

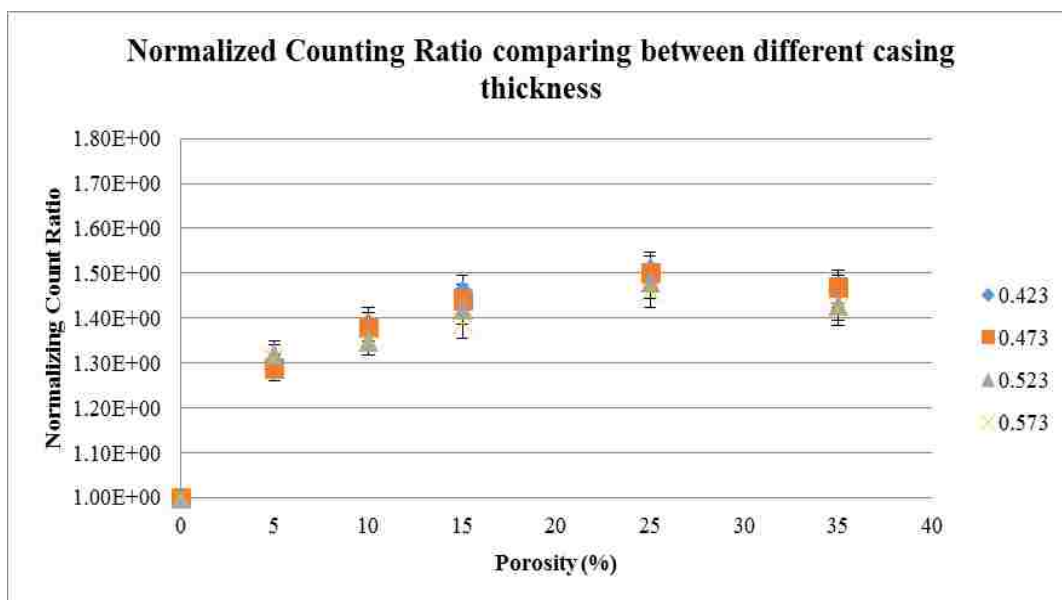


Figure 21: Normalized Count Ratio versus Stainless Steel Thickness

### 3.4.3 Borehole Size Results

Figures 22 and 23 show variation of photon counts versus porosity using different borehole sizes for near and far detectors, respectively.

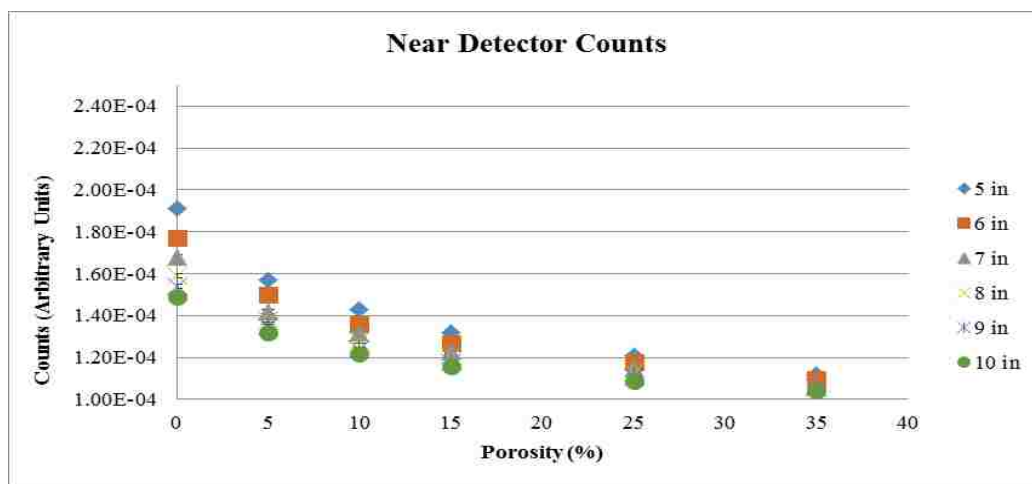


Figure 22: Count Rate versus Porosity and Borehole Size, Near Detector

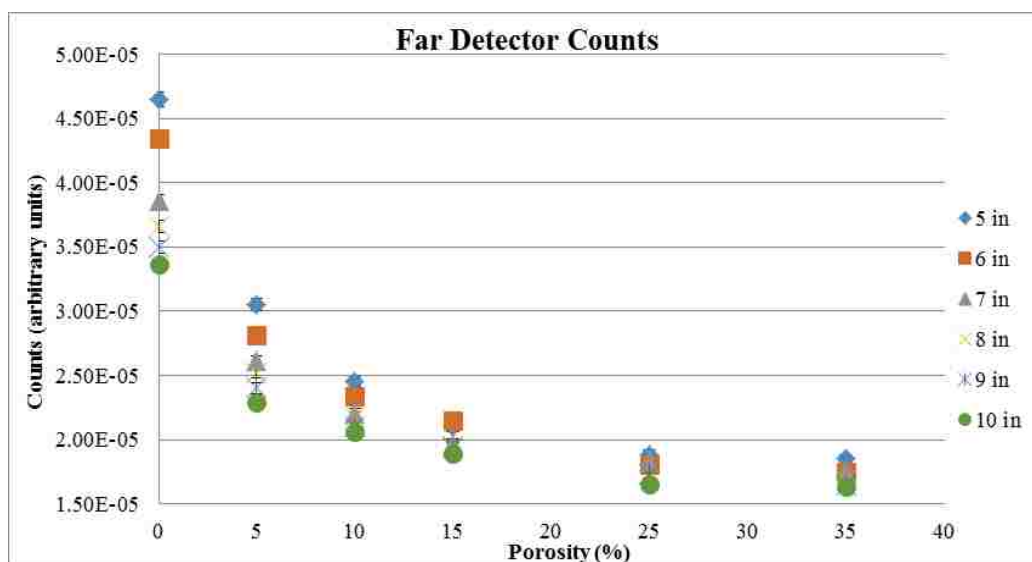


Figure 23: Count Rate versus Porosity and Borehole Size, Far Detector

Figure 24 shows the normalized Count ratio versus porosity using different borehole sizes in cases of near to far detectors.

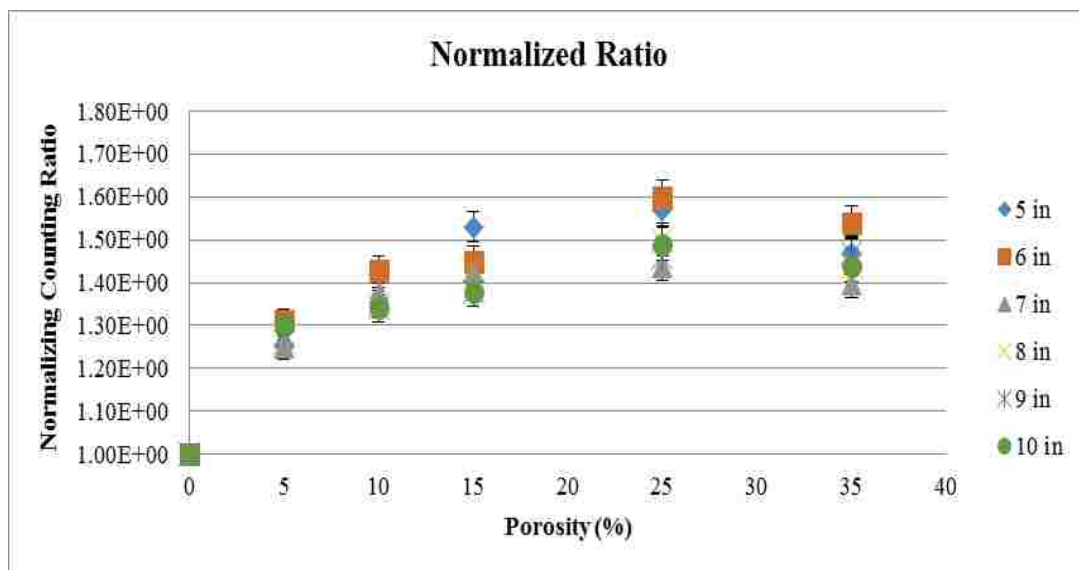


Figure 24: Normalized Count Ratio versus Borehole Size

### 3.4.4 Temperature Results

Figures 25 and 26 show the variation of photon counts rate versus temperature in cases of near and far detectors, respectively.

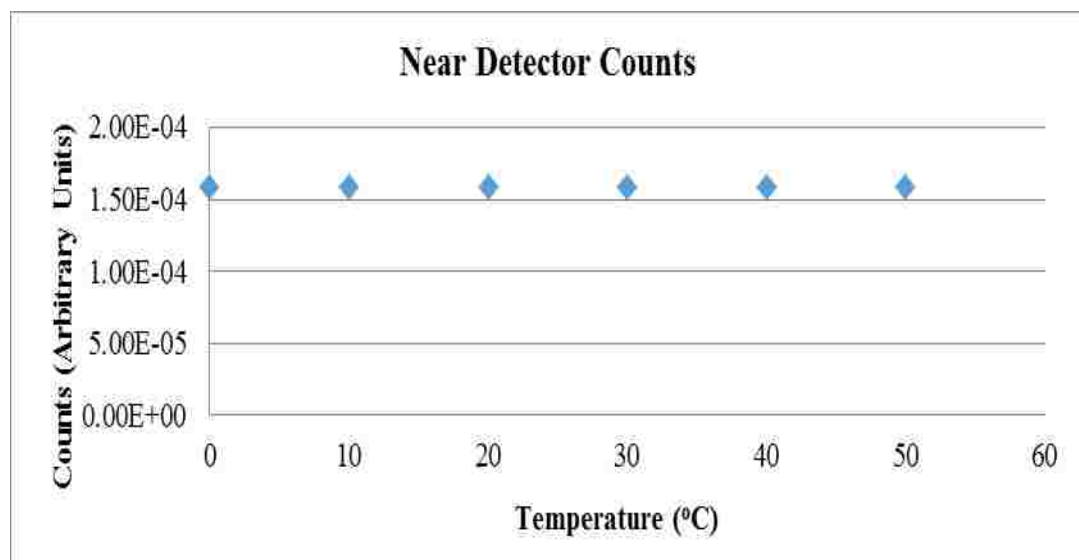


Figure 25: Counts Rate versus Temperature, Near Detector



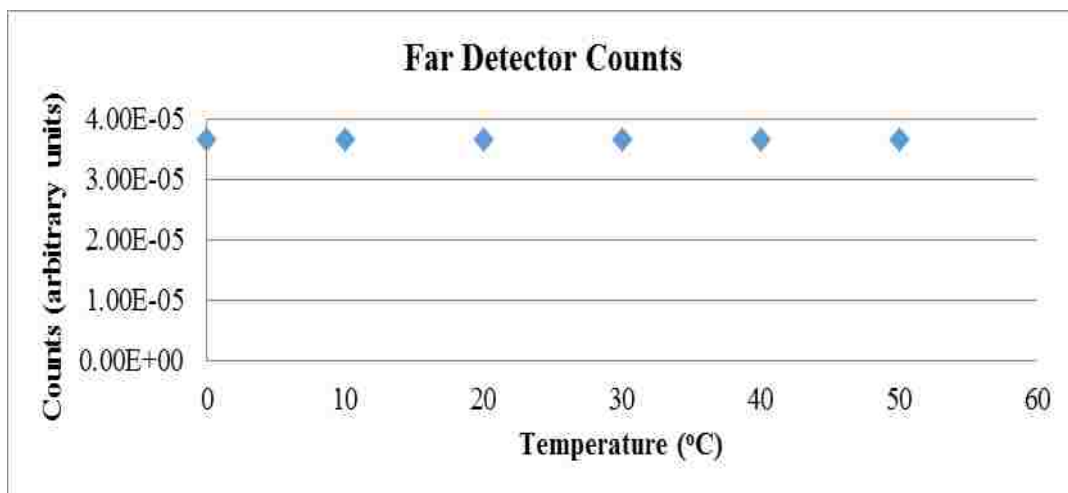


Figure 26: Counts Rate versus Temperature, Far Detector

### 3.4.5 Cross Section Results

From the Evaluated Nuclear Data File (ENDF) system, using two specific libraries 60c (1977) and 70c (2003), data about the cross section is available for various isotopes and elements at the same temperature 293.6 °K (see Table G.2 in Appendix G of the MCNP manual [55]). Figures 27 and 28 show the number of photons versus porosity for various libraries 60c and 70c in cases of near and far detectors, respectively.

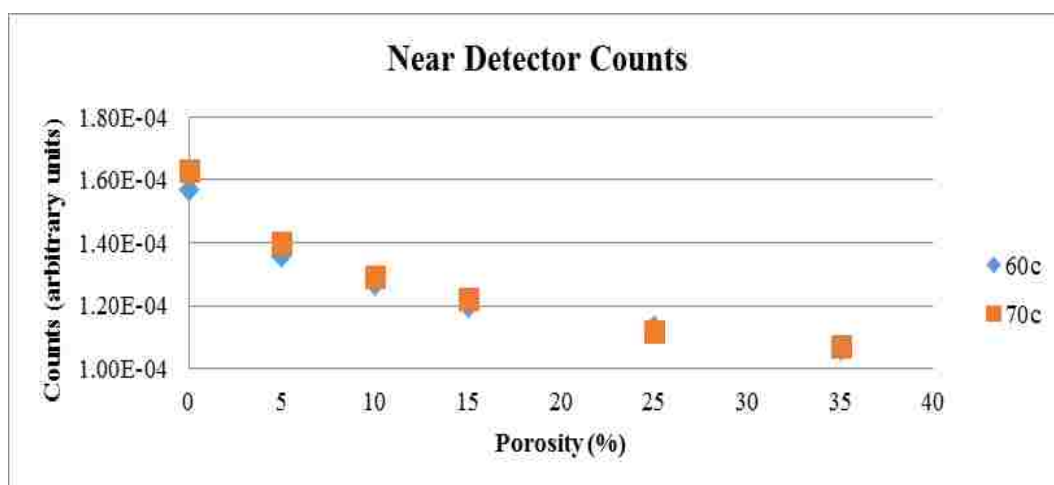


Figure 27: Near Detector Counts versus Porosity for Two Different Cross Sections

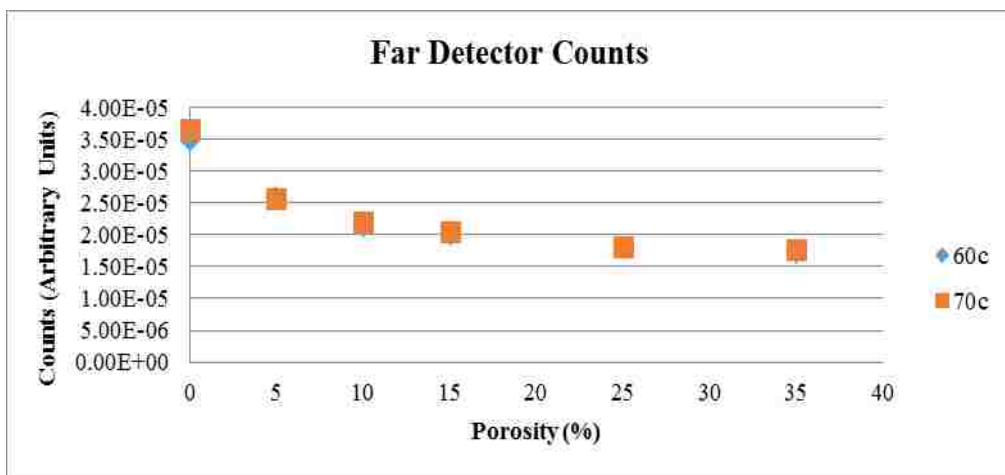


Figure 28: Far Detector Counts versus Porosity for Two Different Cross Sections

Figure 29 show normalized ratio of the near to far detectors counts versus porosity for two libraries (60c and 70c) cross sections.

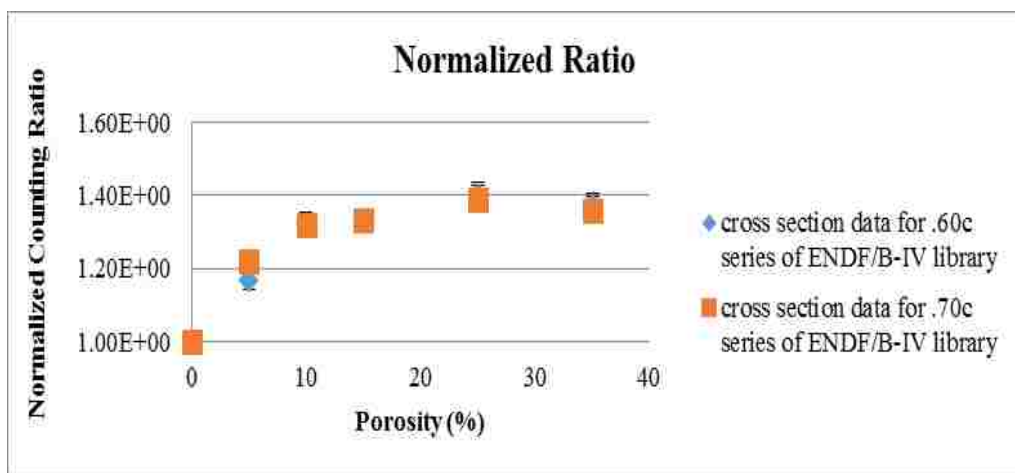


Figure 29: Normalized Counting Ratio versus Porosity for Two Different Cross Sections

### 3.4.6 Borehole Salinity Results

Table 6 shows the relation between water saline density and salinity. Obviously there is a linear relationship between salinity and its density.

Table 6: Density of Saline Water versus Salinity

Salinity (%)	Saline water density (g/cm <sup>3</sup> )
0	1.00
5	1.0276
10	1.0569
15	1.0878
20	1.1206
25	1.1554
30	1.1925

Figures 30 and 31 show the photon counts versus salinity using different porosity values (namely porosity values are: (0%, 5%, 15%, 25%) in cases of near and far detectors. They illustrate the effects of saline water in the borehole on the combined tool sensitivity. Figure 32 shows the normalized count ratio versus salinity using four different values of porosity.

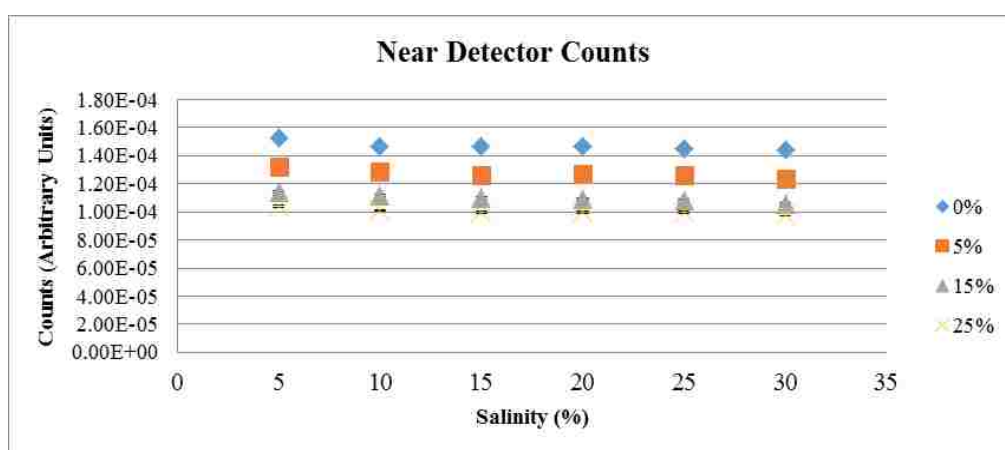


Figure 30: Near Detector Counts, Borehole Salinity

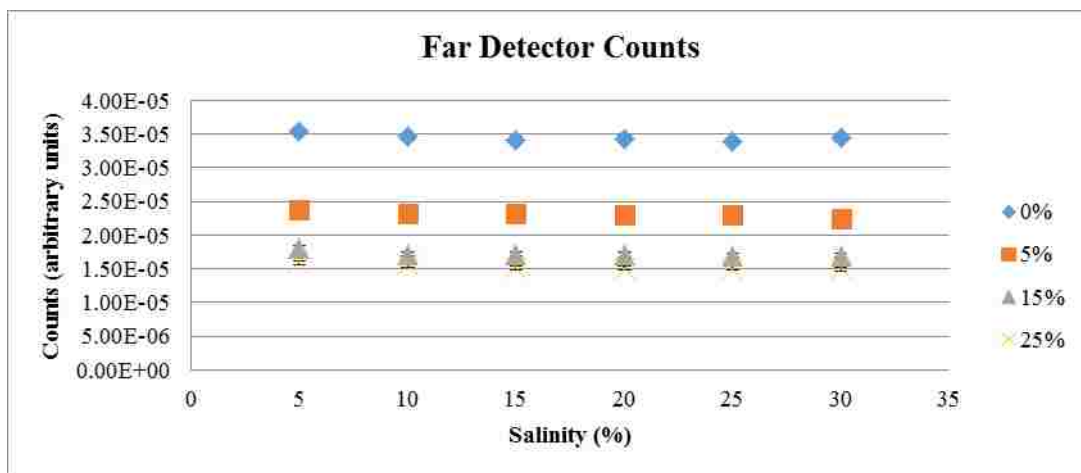


Figure 31: Far Detector Counts, Borehole Salinity

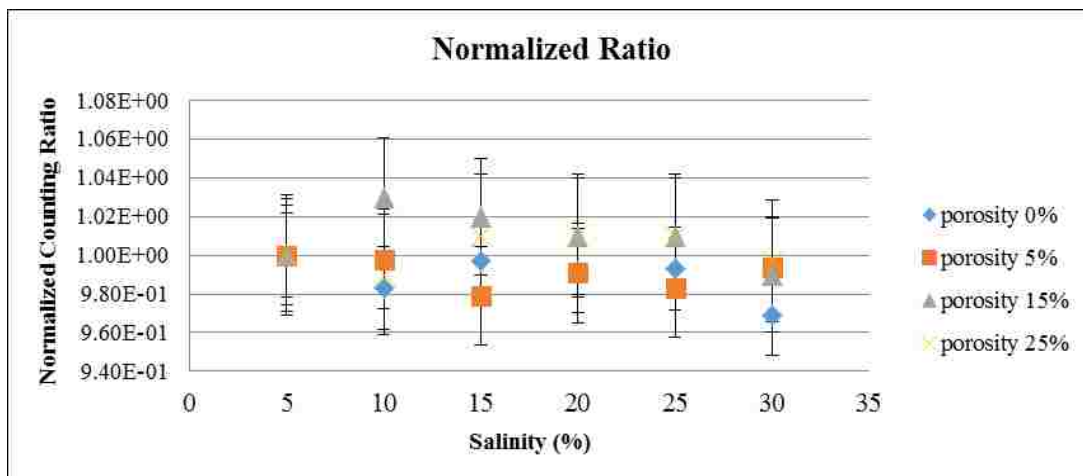


Figure 32: Normalized Counting Ratio, Borehole Salinity

### 3.4.7 Formation Salinity Results

Table 7 shows the relationship between density of the formation and salinity at different values of porosities. Table 7 reveals that the density of the formation increases with the increasing salinity; but the formation density decreases with the increasing porosity.

Table 7: Formation Density versus Salinity and Porosity

Salinity (%)	Formation density (g/cm <sup>3</sup> ) at porosity	Formation density (g/cm <sup>3</sup> ) at porosity	Formation density (g/cm <sup>3</sup> ) at porosity
	5%	15%	25%
5	2.6268	2.4585	2.2901
10	2.6283	2.4629	2.2974
15	2.6298	2.4675	2.3052
20	2.6315	2.4724	2.3134
25	2.6332	2.4777	2.3221
30	2.6351	2.4832	2.3314

As it is well known, chlorine and sodium in the saline water have more absorption cross section than the hydrogen in the pure water (31.6, 0.505, 0.30 barns corresponding to Cl, Na, and H, respectively)[56]. Figures 33 and 34 display the photon counts versus salinity for near and far detectors at different values of formation porosity 0%, 5%, 15%, and 25%. Figure 35 shows normalized count ratio versus salinity using four different values for porosity.

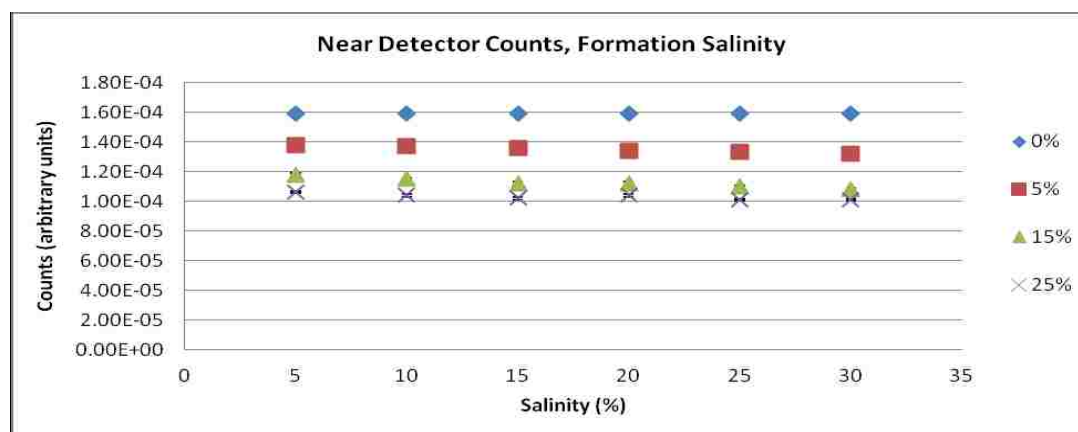


Figure 33: Near Detector Counts, Formation Salinity

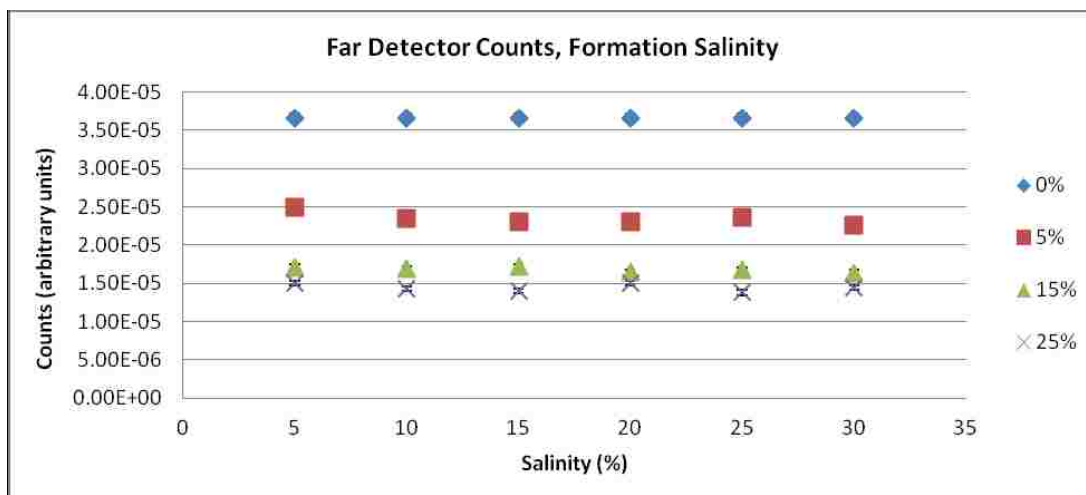


Figure 34: Far Detector Counts, Formation Salinity

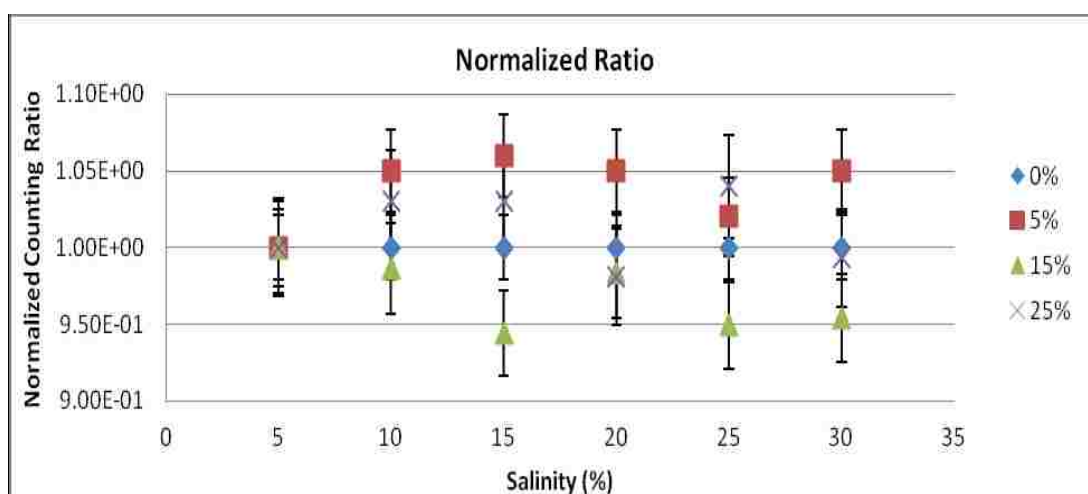


Figure 35: Normalized Counting Ratio, Formation Salinity

### 3.4.8 Boron Thickness Results

After making change in Boron thickness at these values (0.05 cm, 0.1 cm, 0.15 cm, 0.2 cm, 0.25 cm, 0.3 cm, 0.35 cm), Figures 36 and 37 show photons count versus porosity at different values of Boron thickness in the cases of near and far detectors, respectively.

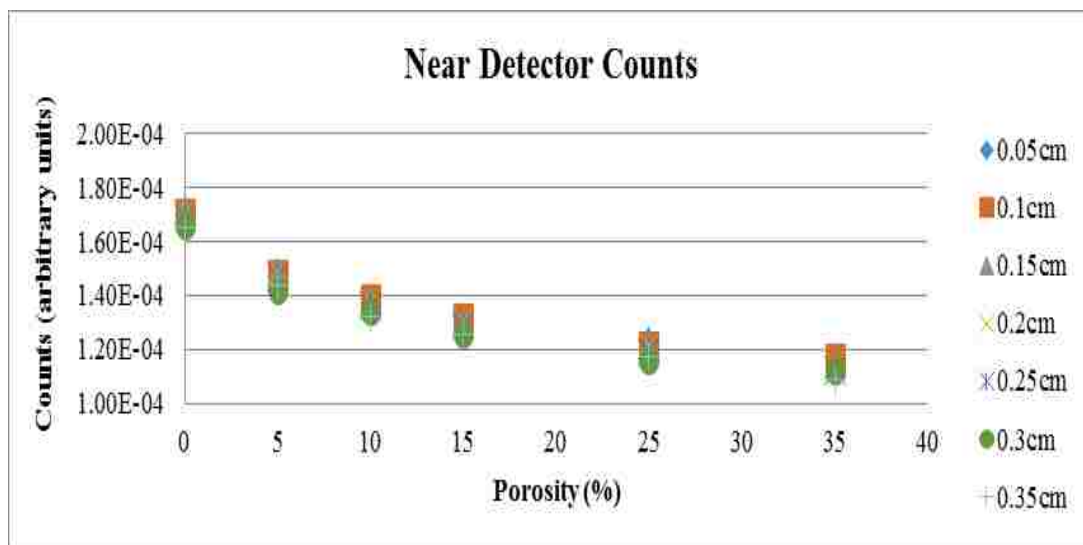


Figure 36: Photons Counts versus Porosity and Boron Thickness, Near Detector

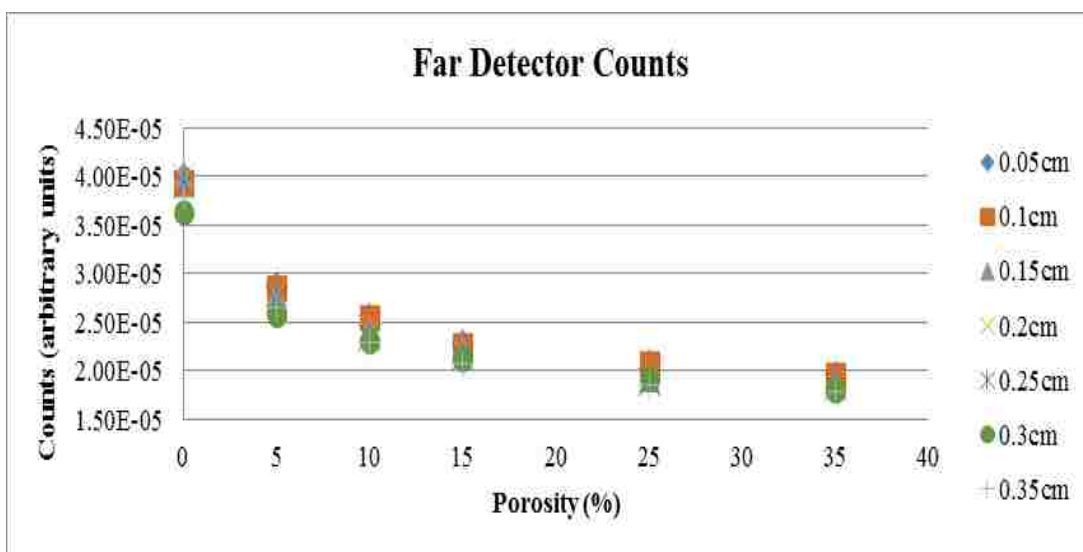


Figure 37: Photons Counts versus Porosity and Boron Thickness, Far Detector

Figure 38 displays the Normalized Ratio of the near to far detectors counts at the variety of the boron thickness.

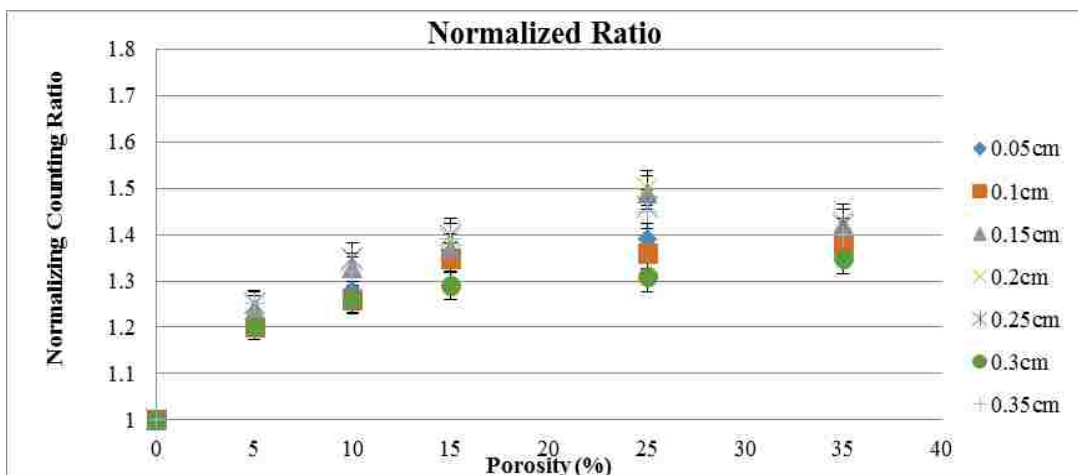


Figure 38: Normalized Count Ratio versus Porosity and Boron Thickness

### 3.5 Sensitivity Results

Figures (39-45) show the sensitivity ratio as a function of porosity for the factors that would have effects on the combined tool response (i.e., the source-to-detector spacing, casing, borehole size, cross section, borehole salinity, formation salinity and the boron thickness. The sensitivity ratios are as follows:

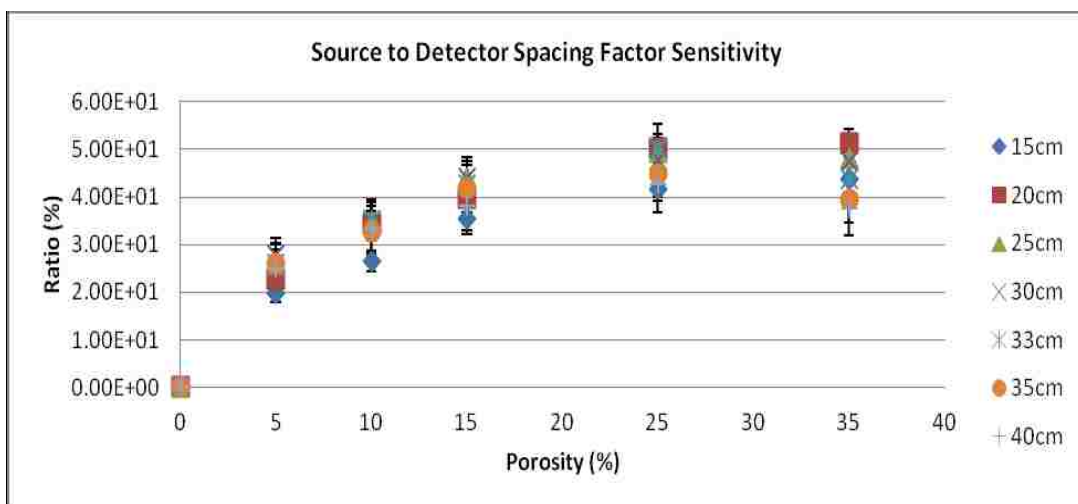


Figure 39: Sensitivity Factor versus Porosity and the Source-to-Detector Spacing



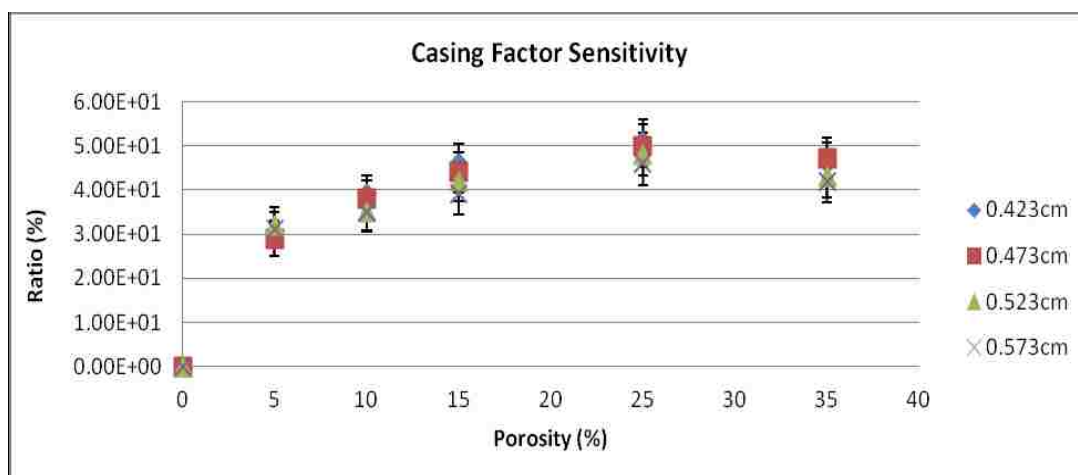


Figure 40: Sensitivity versus Porosity and Casing Factor

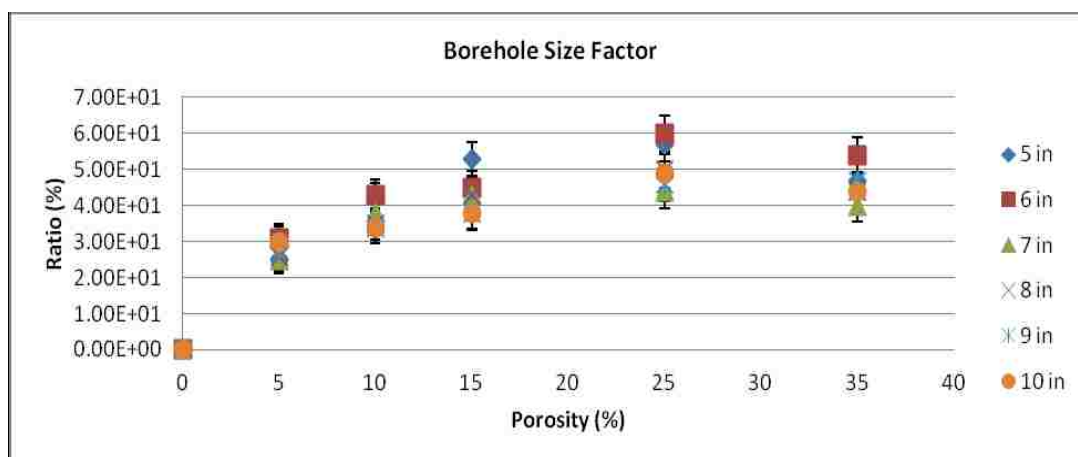


Figure 41: Sensitivity versus Porosity and Borehole Size Factor

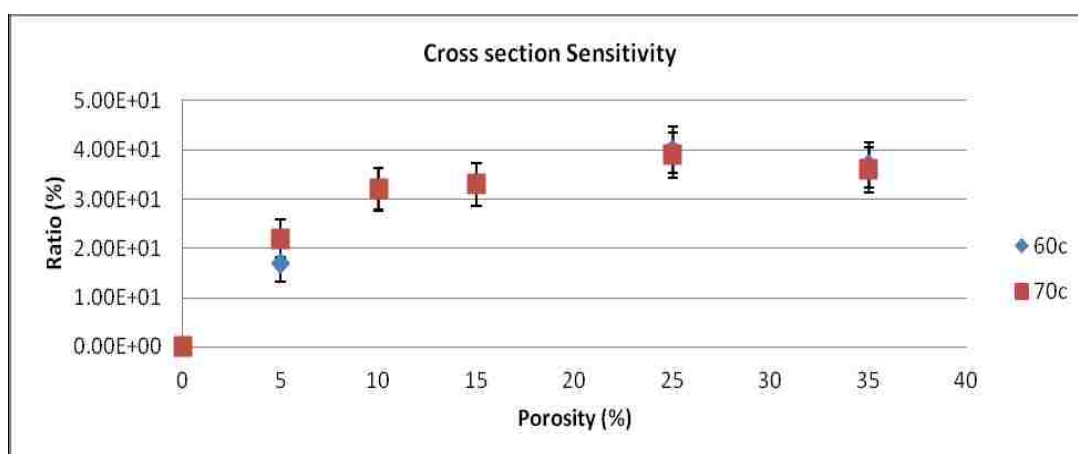


Figure 42: Sensitivity versus Porosity and Cross Section Factor

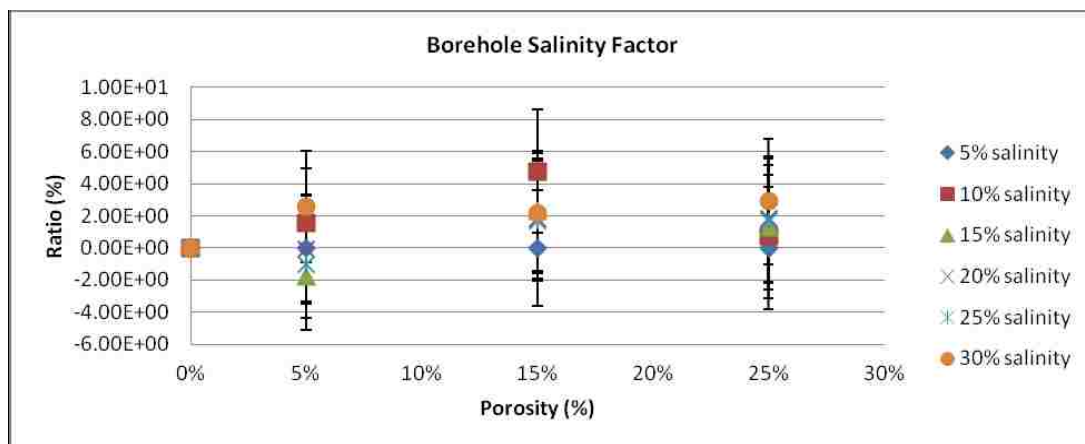


Figure 43: Sensitivity versus Porosity and Borehole Salinity Factor

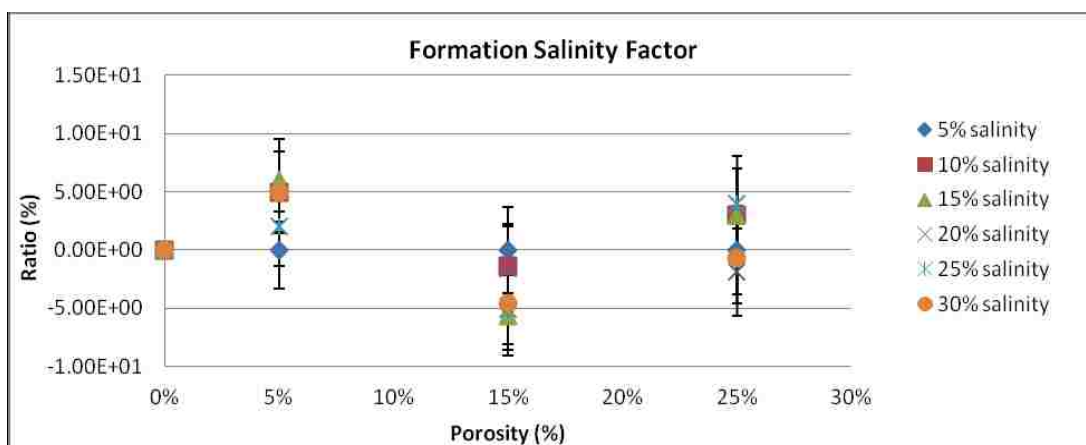


Figure 44: Sensitivity versus Porosity and Formation Salinity Factor

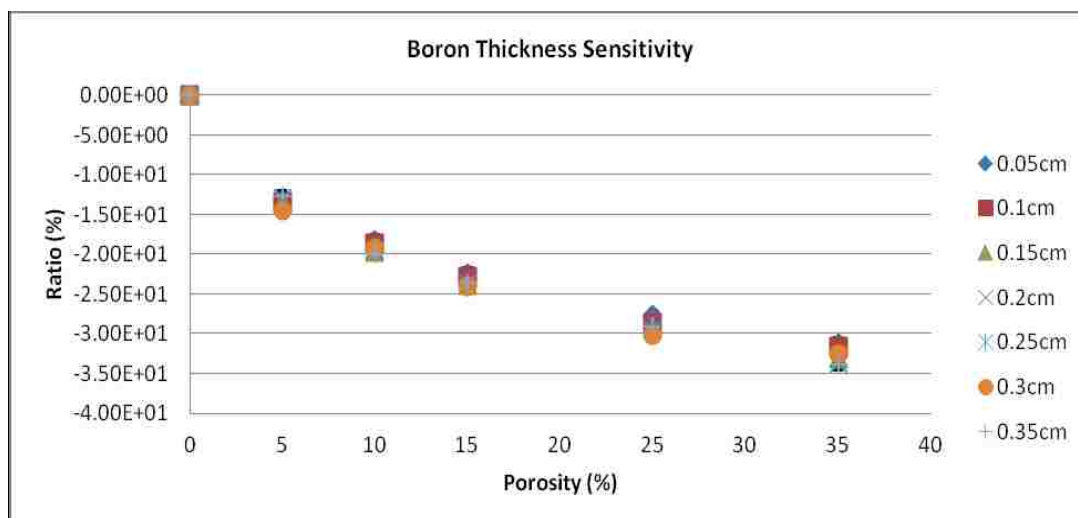


Figure 45: Sensitivity versus Porosity and Boron Thickness Factor

## Chapter 4: Discussion

### 4.1 Interpretation of the Effect of the Porosity on the Combined-Tool Response

In limestone (Calcium carbonate “CaCO<sub>3</sub>”)-based detectors having pores filled with (saline) water, which 2/3 of its composition is hydrogen atoms, possess the ability to thermalize fast neutrons. This usually takes place because the hydrogen atom has approximately the same mass of neutron and any type of scattering events would yield a reduction of kinetic energy of neutrons. With the increase of porosity the number of hydrogen atoms increases resulting in a little amount of thermal neutrons to reach the near detector. On the other hand, the interaction of a thermal neutron with boron would produce gamma rays with energy 0.48 MeV as the collision is inelastic.

It is obvious that boron absorption of neutrons at low energies is very effective. Thus, the number of the produced gamma rays is proportional to the number of the thermal neutrons, which are absorbed in the boron layer. As a matter of fact, the number of absorbed neutrons is proportional to the back-scattered neutrons from the formation which is, in turn, proportional to the porosity. Considering the fact that one detector is placed farther from the source than the other one, so one should expect their detections to thermal neutrons to be different (i.e., the closer the detector the more neutrons are detected).

Figures 7 and 8 show the detector counts versus porosity. That is to say, when porosity increases the count rate decreases, which suggests that both detectors are more sensitive at small values of porosity.

Thus, the additional thermalization of neutrons will lead to some neutrons being absorbed in the formation and not reaching the far detector. Comparing these results with Figures 3 and 4 [15], strong correlations are observed between them with little increase in the count rate values in Figures 7 and 8 of this research. This minor difference can be attributed to the fact that in Figures 3 and 4 [15] the boron lined directly on the detector, whereas in our present work Aluminum is used directly on the detector. Then the amount of thermal neutron will be lost through the moderators, as Aluminum is heavier than boron.

Figure 9 in this work and Figure 5 [15] show the normalized ratio of the near to far detector count rates versus porosity. Both Figures agree to suggest that the effective sensitivity should be achieved at small values of porosity. In relation to Figure 6 [33] the exact behavior is evident in Figure 9 in this research. In addition to that, correlation with Figures 5 and 7 [29,31] is also noticed at high level. Not only that, but also Figure 5 [57], and Figure 6 [58] are all in good agreement.

#### **4.2 Interpretation of the Reduction of the Incident Neutron Flux on the Detectors**

Figures (10-15) show F1-tally which represents the neutron current incident on the near and far detectors with and without boron lining for use in thermal, epithermal, and fast neutron energy range. When compared with Figures 6 and 7 [15], the boron lining appears to be a better absorber of thermal neutrons than it does for epithermal and fast neutrons. The cross section of neutron in the boron as in ENDF/B-VI are displayed (32188.45b, 109.3645b, 3.044419b), respectively [59]. Displaying a great reduction in counts versus kinetic energy of neutrons incident on the detectors, Figure 4 [21] is in support of the trends.

### **4.3 Interpretation of Factors Affecting the Combined Tool Response**

#### **4.3.1 Source-to-Detector Spacing Factor Results**

Fast neutron emitted from the source with high energy (14 MeV) moves through different materials to finally reach the detector. Some materials act as moderator materials, in which the neutron undergoes an interaction either scattering or absorption. Decreasing the neutron source-detector distance increases the count rate. Obviously, as the source-to-detector distance decreases more neutrons get thermalized and thus more neutrons get absorbed in the formation. So, the count should increase with the decreasing source-to-detector distance. Figure 2 [37] agrees favorably with Figure 16 of this research.

Figures 16 and 17 show the counting rate decreasing with the increasing porosity at all the values of the source-to-detector distance for both near and far detectors, respectively. The sensitivity of the combined tool response decreases with increasing the porosity, and decreases with increasing the space between the source and the detector as shown in figure 39. Figure 18 confirms that the combined tool is more sensitive at small values of porosity, and counting rate decreases with increasing source-to-detector distance. In comparing the near to far detector counting rate as in Figures 16 and 17 the number of photons which are detected by far detector is less than the number of photons detected by near detector. That is to say, the neutrons which are emitted from the source will undergo more absorption events in the formation and may not all reach the far detector. A good agreement between Figure16 in this study with Figures 1 [24], and Figure 20 [35] is noticeable.

### **4.3.2 Casing (Stainless Steel) Thickness Factor Results**

Stainless steel has both a high density and a high average atomic number, which have an impact on increasing the attenuation coefficient. The mean free path of the thermal neutron absorption cross section in stainless steel is about 0.042cm.

With increasing stainless steel thickness, the neutrons are expected to have more interaction with nuclei and might be completely attenuated before reaching the boron layer. This would lead to a decrease in the count rate with increasing stainless-steel thickness as shown in Figures 19 and 20.

Figures 19 and 20 show the count rate decreases with the increasing porosity, which indicate that the detector is more sensitive at small values of porosity and both near and far detectors are a bit sensitive to the casing (stainless-steel) thickness. Figure 21 confirms that trend as well. Figure 40 indicates that the combined tool is more sensitive at small values of porosity, and decreases with increasing the casing as shown by the results of the sensitivity ratio.

### **4.3.3 Borehole Size Factor Results**

When increasing borehole size, in borehole filled with water, the water size increases. Knowing that water is a good moderator material as it contains hydrogen atoms, then the increase in borehole size would cause a reduction in photon count rate, as more thermalization can take place with the available hydrogen atoms. Figures 22 and 23 show that trend that count rate decreases with borehole size and especially in the region of low porosity as the sensitivity should be at its best. Figure 24 of normalized ratio of the near to far detectors' counts versus porosity at different borehole sizes also confirms that as well with high resolution in high-to-intermediate

porosity. Moreover, borehole size have more effect on near detector than it does on far detector because thermalization of more efficient in the first one. The borehole size seems to have more effect than the formation because of being placed closer to the source and detectors. Figure 41 shows a high sensitivity of the borehole size at small values of porosity, and also that the sensitivity decreases with increasing the borehole size.

#### **4.3.4 Temperature Factor Results**

The attention given to the temperature is only to affect the speed of nucleus. The temperature turned out to have a very limited effect on the obtained results. This is revealed on having no change in the counts at various temperature values, as displayed in Figures 25 and 26, which show the counts versus temperature for near and far detectors, respectively.

#### **4.3.5 Cross Section Factor Results**

For different cross section values, found in series 70c and 60c in ENDF library, insignificant change of count is obtained. The same trend is confirmed for thermal epithermal and fast neutron, using the cross section values in 70c, and 60c series, (30902.58 b, 116.9155 b, 2.978656 b), (32188.45 b, 109.3645 b, 3.044419 b)[59], respectively. Figures 27 and 28 show clearly this trend that the cross section has negligible effect on sensitivity. Figure 29 confirms that as well it shows a bit high sensitivity in 60c series as show in Figure 42.

#### **4.3.6 Borehole Salinity Factor Results**

Chlorine and sodium have high absorption cross sections that would lead to the reduction of count rate The absorption of thermal neutron cross section of the Cl

is 33.5 b, Na is 0.530 b, and H is 0.3326 b [60]. Figures (30-32) show counts decreasing with increasing porosity, as usual, whereas salinity has minimal effect on counts. According to different values of formation porosity the figures do not show any significant effect. The effect is even negligible in the region of small values of porosity; besides that there is no clear sensitivity effect at small values of porosity (see Figure 43).

#### **4.3.7 Formation Salinity Factor Results**

Figures (33-35) show a decrease in counts with increasing porosity but little decrease with salinity. When increasing salinity, hydrogen is decreased whereas chlorine and sodium increased. Chlorine and sodium have high absorption cross sections, which would lead to a reduction in count rate. Nonetheless, our results show that salinity has a very small effect. Besides, there is no clear sensitivity effect at low values of the porosity as shown in Figure 44.

#### **4.3.8 Boron Thickness Factor Results**

From section 2.7 equation (2), it is clear that the increase in the casing thickness would yield an increase in the number of emitted photons. However, increasing the boron thickness will also lead to more gamma rays attenuation in the boron layer (i.e., the larger the casing thickness the greater the attenuation). Meanwhile, the number of transmitted neutrons decreases with the increasing of the absorption thickness.

Figures 36 and 37 confirm what was suggested by equation (2). These figures show that when increasing boron thickness the counts decrease. Figure 38 shows the normalized ratio as a function of porosity at different boron thickness. Figure 45



shows the sensitivity ratio at different values of boron thickness, corresponding to different values of porosity. Boron thickness is found to be more sensitivity at low values of the porosity and the sensitivity decreases with increasing boron thickness.

## Chapter 5: Conclusion

Using the Monte Carlo N-Particle (MCNP) simulation package, which was originally developed in Los-Alamos National Lab, we have carried out an investigation to optimize neutron and gamma photon detection for impact or application in oil-well logging tool. Initially, we suggested to combine the thermal-neutron-porosity Logging tool with the carbon/oxygen (C/O) Logging tool into so-called “Combined Logging Tool”. Assessments of several factors on the sensitivity of the detector have been carried out, namely: (i) source-to-detector distance, (ii) lining thickness, (iii) borehole size, (iv) borehole salinity, (v) temperature, (vi) capture cross-section, and (vii) the casing (stainless steel) thickness. During the whole investigation, we used two detectors: one near detector at a distance from the source of about 33 cm and one far detector further away from the near-detector by a distance of 28 cm. The source is responsible to emit fast neutrons of energy 14 MeV. As a moderate material, we use stainless steel for casing. The formation consists of limestone ( $\text{CaCO}_3$ ) with pores, of various sizes, filled with saline water. In order to save time and money, boron lining replacement is used to absorb “thermal neutrons” then produce a gamma of energy 0.48 MeV. We have done benchmarking of our results with the existing ones in the literature and especially those due to Metwally [15]. The results show that the combined tool is very sensitive to the porosity under the influence of these factors, especially at small values of porosity

Last but not least, our investigation has shown that the detection is independent of heat.

## References

- [1] Well Logging Tools & Techniques (Porosity Logs). (2009). Retrieved from petroleum, crude oil: <http://petroleumcrudeoil.blogspot.ae/2008/11/well-logging-tools-techniques-porosity.html>
- [2] Well logging. (2016, September 19). Retrieved from Wikipedia: [https://en.wikipedia.org/wiki/Well\\_logging](https://en.wikipedia.org/wiki/Well_logging)
- [3] D. V. Ellis and J. M. Singer, "Well Logging for Earth Scientists", 2<sup>nd</sup> Ed (Springer, Netherlands, 2007).
- [4] Wenbao, J., Can, C., Daqian, H., Yongsheng, L., Hongtao, W., & Da, C. (2015, October 10). Method for correcting thermal neutron self-shielding effect for aqueous bulk sample analysis by PGNAA technique. *J Radioanal Nucl Chem*, 1133–1137
- [5] M. A. Andersen, "Discovering the Secrets of the Earth," Schlumberger, 2011.[Online].Available:file:///C:/Users/SuperB/Downloads/defining\_logging%20(1).pdf.
- [6] "PetroWiki," Society of Petroleum Engineers, 6 July 2015. [Online]. Available: [http://petrowiki.org/Types\\_of\\_logs](http://petrowiki.org/Types_of_logs).
- [7] D. McKeon, "Random Walk Engineering," 26 March 2017. [Online]. Available: <https://www.linkedin.com/in/don-mckeon-891a3225>
- [8] R. D. Felder, "Cased-Hole Logging for Evaluating Bypassed Reserves," *Journal of Petroleum Technology*, Vol. 40, pp. 969-973, 1988.
- [9] N. Tsoufanidis and S. Landsberger, "Measurement & Detection of Radiation", (CRC Press, Taylor & Fransics Group, Boca Raton, London, 2015).
- [10] K. A. McConnell, "14 MeV Neutron Generator Dose Modeling," Texas, 2013.
- [11] B. Donmez, "Characterization of Single-Sided CdZnTe Strip Detectors for High Energy Astrophysics Applications," PhD Thesis (University of New Hampshire, 2006).

- [12] R. E. Schmitz, A. M. Alessio and P. E. Kinahan, "The Physics of PET/CT scanners", <http://radiologykey.com/the-physics-of-petct-scanners/>
- [13] E. Shaw, "Instruments for Radiation Detection and Measurement Lab # 3," [Online]. Available: <http://slideplayer.com/slide/5685855/>. [Accessed 27 March 2017].
- [14] "How Do Sodium Iodide Scintillation Detectors Work," Nevada Technical associates, 10 September 2015. [Online]. Available: <http://www.ntanet.net/how-do-sodium-iodide-scintillation-detectors-work>.
- [15] W. A. Metwally, "Porosity calculations using a C/O logging tool with boron-lined NaI detectors," *Applied Radiation and Isotopes*, Vol. 69, pp. 217–219, 2 August 2010.
- [16] I.M. Sobol, *A Primer for the Monte Carlo Method*, Boca Raton: CRC Press, 1994. <https://archive.org/details/APrimerForTheMonteCarloMethod>.
- [17] K. Teknomo, "Monte Carlo Simulation Tutorials," 2016. [Online]. Available: <http://people.revoledu.com/kardi/tutorial/Simulation/index.html>.
- [18] P. Parvaresh and M. Sohrabpour, "Design and testing of a neutron porosity probe using MCNP code," *Journal of Radioanalytical and Nuclear Chemistry*, Vol. 260, pp. 335-337, 10 July 2004.
- [19] A. Drabina, T. Zorski and U. Woźnicka, "Correlation between Measurements and Monte-Carlo Calculations for the NNTE Logging-Tool," University of Mining and Metallurgy, Poland, 2003. [www.ifj.edu.pl/reports/2003.html](http://www.ifj.edu.pl/reports/2003.html)
- [20] N. Chikhradze, F. Marquis, G. Abashidze and L. Kurdadze, "Development and Performance of New Gadolinium and Boron Containing Radiation-Absorbing Composite Systems," *Journal of Minerals, Metals & Materials Society (TMS)*, Vol. 65, pp. 728-738, 23 April 2013.
- [21] J. Liu, F. Zhang, X. Wang, F. Han and Z. Yuan, "Numerical study on determining formation porosity using a boron capture gamma ray technique and MCNP," *Applied Radiation and Isotopes*, Vol. 94, p. 266–271, December 2014.

- [22] W. A. Metwally, "Existing NaI detectors; an efficient alternative to He-3 detectors," *Nuclear Instruments and Methods in Physics Research Section B: Beam Interactions with Materials and Atoms*, Vol. 338, pp. 48–51, 1 November 2014.
- [23] L. Swiderski, M. Moszynski, D. Wolski, J. Iwanowska, T. Szczesniak, G. Pausch, C. Plettner, J. Stein, P. Schotanus, C. Hurlbut and J. Szabelski, "Comparison of Neutron Detection Efficiency of a He-3 Counter and a Boron-10 Loaded Liquid Scintillator," *IEEE Transactions on nuclear science*, vol. 57, pp. 2857-2861, 2010.
- [24] M. Shahriari and M. Sohrabpour, "Borehole parametric study for neutron induced capture  $\gamma$ -ray spectrometry using the MCNP code," *Applied Radiation and Isotopes*, Vol. 52, p. 127–135, January 2000.
- [25] F. Li and X. Han, "Implementation of a tree algorithm in MCNP code for nuclear well logging applications," *Applied Radiation and Isotopes*, Vol. 70, p. 1063–1069, July 2012.
- [26] S. Korotkin, U. Wengrowicz and I. Orion, "Detection unit optimization of a neutron searching detector using Monte Carlo Simulations," *Nuclear Instruments and Methods in Physics Research Section A: Accelerators, Spectrometers, Detectors and Associated Equipment*, Vol. 660, p. 154–161, 21 December 2011.
- [27] E. Akaho, S. Jonah, C. K Dagadu, B. Maakuu, P. Adu, S. Anim-Sampong and A. Kyere, "Geometrical effects on thermal neutron reflection of hydrogenous moderators using  $^{241}\text{Am}$ -Be source," *Applied Radiation and Isotopes*, Vol. 55, p. 175–179, August 2001.
- [28] J. Fantidis, G. Nicolaou, C. Potolias, N. Vordos and D. Bandekas, "The comparison of four neutron sources for Prompt Gamma Neutron Activation Analysis (PGNAA) in vivo detections of boron," *Journal of Radioanalytical and Nuclear Chemistry*, Vol. 290, pp. 289–295, 17 July 2011.

- [29] C. R. Peeples, M. Mickael and R. P. Gardner, "On replacing Am–Be neutron sources in compensated porosity logging tools," *Applied Radiation and Isotopes*, Vol. 68, p. 926–931, April–May 2010.
- [30] A. Chen, A. Antolak and K.-N. Leung, "Electronic neutron source for compensated porosity well logging," *Nuclear Instruments and Methods in Physics Research A: Spectrometers, Detectors and Associated Equipment*, Vol. 684, pp. 52-56, 25 August 2012.
- [31] J. Liu, F. Zhang, R. Gardner, G. Hou, Q. Zhang, Y. Zhang, X. Li, H. Li and C. Hu, "A method to improve the sensitivity of neutron porosity measurement based on D-T source," *Journal of Natural Gas Science and Engineering*, Vol. 33, pp. 879-884, 2016.
- [32] H. R. Vega-Carrillo, E. Manzanares-Acuña, A. M. Bacerra-Ferreiro and A. Carrillo-Nuñez, "Neutron and gamma-ray spectra of  $^{239}\text{PuBe}$  and  $^{241}\text{AmBe}$ ," *Applied Radiation and Isotopes*, Vol. 57, p. 167–170, August 2002.
- [33] M. Rasoulinejad, R. I. Najafabadi and N. Ghal-Eh, "A Simple Well-Logging Tool Using Boron-Lined Sodium Iodide Scintillators and an Neutron Source," *Radiation Protection Dosimetry*, Vol. 151, p. 80 – 585, 20 March 2012.
- [34] W. Wu, M. Tong, L. Xiao and J. Wang, "Porosity sensitivity study of the compensated neutron logging tool," *Journal of Petroleum Science and Engineering*, Vol. 108, pp.10–13, August 2013.
- [35] L. M. Scallan, "Efficiency Modeling for Neutron Detectors," MSc. Thesis (Colorado State University, Fort Collins, Colorado, 2014).
- [36] I. Akkurt, K. Gunoglu and S. Arda, "Detection Efficiency of NaI(Tl) Detector in 511–1332 keV Energy Range," *Science & Technology of Nuclear Installations*, Vol. 2014, ID# 186798, pp.1-5, March 2014.
- [37] D.I. Igwesi, "Investigation Of The Effects Of Variation Of Neutron Source-Detector Distance On The Emitted Neutron Dose Equivalent," *Journal of Multidisciplinary Engineering, Science and Technology*, Vol. 2, pp. 1562-1566, June 2015.

- [38] M. Bastürk, J. Arzmann, W. Jerlich, N. Kardjilov, E. Lehmann and M. Zawisky, "Analysis of neutron attenuation in boron-alloyed stainless steel with neutron radiography and JEN-3 gauge," *Journal of Nuclear Materials*, Vol. 341, p. 189–200, 15 May 2005.
- [39] A. Shahri, N. Ghal-Eh and G. Etaati, "Modelling boron-lined proportional counter response to neutrons," *Radiation Protection Dosimetry*, Vol. 156, pp. 349-355, March 2013.
- [40] J. Sun and R. P. Gardner, "Optimization of the steady neutron source technique for absorption cross section measurement by using an  $^{124}\text{Sb}$ –Be neutron source," *Nuclear Instruments and Methods in Physics Research Section B: Beam Interactions with Materials and Atoms*, Vol. 213, p. 22–28, January 2004.
- [41] R. Khelifi, Z. Idiri, L. Omari and M. Seghir, "Prompt gamma neutron activation analysis of bulk concrete samples with an Am–Be neutron source," *Applied Radiation and Isotopes*, Vol. 51, p. 9–13, July 1999.
- [42] W. Jia, C. Cheng, D. Hei, Y. Ling, H. Wang and D. Chen, "Method for correcting thermal neutron self-shielding effect for aqueous bulk sample analysis by PGNAA technique," *Journal of Radioanalytical and Nuclear Chemistry*, Vol. 304, p p. 1133–1137, June 2015.
- [43] F. Al-Shehri, A. Naqvi and A. Ashry, "Elemental Analysis of Coal Samples using PGNAA Technique," *Girls Education College, Dammam*, 31261, Saudi Arabia, pp. 3860-4281, 23 september 2016.
- [44] M. Borsaru, C. Smith, J. Merritt, T. Aizawa and A. Rojc, "In situ determination of salinity by PGNAA," *Applied Radiation and Isotopes*, vol. 64, p. 630–637, May 2006.
- [45] T. Cywicka-Jakiel, "Progress in numerical modelling of the Cl influence on  $\gamma$ -ray spectra from an n-gamma logging tool, by using the improved ENDF data for radiative capture," *Applied Radiation and Isotopes*, Vol. 65, pp. 731–738, June 2007.

- [46] D. Igwesi and O. Thomas, "Determination of thermal neutron macroscopic cross section for two polythene based slabs using monte carlo n-particle code," *Multidisciplinary Engineering Science and Technology*, Vol. 1 pp. 281-284, December 2014. <http://www.jmest.org/wp-content/uploads/JMESTN42350260.pdf>
- [47] H. Qing-Yuan, H. Xin-Miao and W. Geng-Fei, "A New Chlorine Logging Tool: Application In The Oilfield Development With High Salinity Formation Water," *Jiangnan Well Logging Institute*, pp. 184-192.
- [48] M. Oraby, K. Verghese and R. Gardner, "Investigation of an improved-sensitivity neutron- porosity oil-well logging tool," *Nuclear Instruments and Methods in Physics Research Section A; Accelerators, Spectrometers, Detectors and Associated Equipment*, Vol. 299, pp. 674-681, December 1990.
- [49] E. B. Podgorsak, "ComSpringer, pendium to Radiation Physics for Medical Physicists", 3<sup>rd</sup> Ed. (Springer-Verlag, Berlin Heideberg, 2014).
- [50] D. P. Glover, "The Neutron Log in Petrophysics MSc Course Notes, pp. 150-171.[http://homepages.see.leeds.ac.uk/~earpwjg/PG\\_EN/CD%20Contents/GGL-66565%20Petrophysics%20English/Chapter%2015.PDF](http://homepages.see.leeds.ac.uk/~earpwjg/PG_EN/CD%20Contents/GGL-66565%20Petrophysics%20English/Chapter%2015.PDF)
- [51] J.F. Briesmeister, Ed., " MCNP- A General Monte Carlo N-Particle Transport Code, Version 5, Vol. II, California: Los Alamos National Laboraty, 2003.
- [52] "Basic Physics of Nuclear Medicine/Attenuation of Gamma-Rays," 30 May 2016.[Online].Available:[https://en.wikibooks.org/wiki/Basic\\_Physics\\_of\\_Nuclear\\_Medicine/Attenuation\\_of\\_Gamma-Rays#Attenuation\\_Experiment](https://en.wikibooks.org/wiki/Basic_Physics_of_Nuclear_Medicine/Attenuation_of_Gamma-Rays#Attenuation_Experiment).
- [53] G. F. Knoll, "Radiation Detection and Measurement", 3<sup>rd</sup> Ed. (John Wiley & Sons Inc., New York, 2000).
- [54] L. MacDonald, "Counting Statistics and Error Propagation," 10 April 2011. [Online].Available:[http://depts.washington.edu/imreslab/2011%20Lectures/ErrorProp-CountingStat\\_LRM\\_04Oct2011.pdf](http://depts.washington.edu/imreslab/2011%20Lectures/ErrorProp-CountingStat_LRM_04Oct2011.pdf).
- [55] X.-5. M. C. Team, MCNP — A General Monte Carlo N-Particle Transport Code, Version 5, Vol. I, California,: Los Alamos National Laboratory, 2003.



- [56] F. L. Peterson, "Neutron Well Logging in Hawaii," 1974.  
<http://hdl.handle.net/10125/18110>
- [57] C.M. Frankle and G.E. Dale, "Unconventional neutron sources for oil well logging," Nuclear Instruments and Methods in Physics Research Section A: Accelerators, Spectrometers, Detectors and Associated Equipment, Vol. 723, pp. 24-29, 10 September 2013.
- [58] W. Wu, M. Tong, L. Xiao and J. Wang, "Porosity sensitivity study of the compensated neutron logging tool," Journal of Petroleum Science and Engineering, Vol. 108, pp. 10-13, 24 August 2013.
- [59] V. Zerkin, "Evaluated Nuclear Data File (ENDF)," 10 March 2017. [Online]. Available: <https://www-nds.iaea.org/exfor/endl.htm>.
- [60] V. F. Sears, "Neutron scattering lengths and cross section," Journal of Neutron News, Vol. 3, pp. 26-37, August 2006.

Shriee  
n

Digitally signed by Shrieen  
DN: cn=Shrieen, o=UAEU,  
ou=Libraries Deanship,  
email=shrieen@uaeu.ac.ae,  
c=AE  
Date: 2017.07.17 11:00:04  
+04'00'